J. Physiol. (1987), **385**, *pp.* 207–242
With 1 plate and 19 text-figures
Printed in Great Britain

VARIATION OF MEMBRANE PROPERTIES IN HAIR CELLS ISOLATED FROM THE TURTLE COCHLEA

BY J. J. ART* AND R. FETTIPLACE

From the Physiological Laboratory, University of Cambridge, Cambridge CB2 3EG

(*Received 1 July 1986*)

SUMMARY

1. Hair cells were enzymatically isolated from identified regions of the turtle basilar papilla and studied with the patch-electrode technique. The experimental aim was to relate the resonance properties seen during current injection to the membrane currents measured in the same cell under whole-cell voltage clamp.

2. Solitary hair cells had resting potentials of about −50 mV, and produced a damped oscillation in membrane potential at the onset and termination of a small current step; the resonant frequency varied from 9 to 350 Hz between cells, and was correlated with the region of papilla from which a cell had been isolated. The inferred frequency map was consistent with the tonotopic arrangement described previously in the intact papilla.

3. Depolarizations from the resting potential under voltage clamp activated a large net outward current with a steep voltage dependence, and the steady-state current–voltage relationship was strongly rectified about the resting potential. Input resistances tended to be smaller in cells with higher resonant frequencies, although there was no concurrent variation in membrane area as inferred from the cell capacitance.

4. The kinetics of the outward current evoked by a small depolarizing step depended upon the resonant frequency, f_0, of the hair cell, and were slower in low-frequency cells. On repolarization to the resting potential the current decayed exponentially with a time constant that changed from 150 ms in the lowest-frequency cell to less than 1 ms in the highest-frequency one. The time constant was approximately proportional to $1/f_0^2$.

5. Following repolarization to different membrane potentials, the tail current was found to reverse around −80 mV, indicating that the outward current was due mainly to K^+.

6. The outward current was abolished by extracellular application of 25 mM-tetraethylammonium chloride (TEA), or on exchange of Cs^+ for K^+ in the intracellular medium filling the recording electrode, each experiment supporting the contention that K^+ is the major current carrier. Such treatments also removed the oscillations in membrane potential evoked by imposed current steps.

7. Addition of TEA or intracellular perfusion with Cs^+ also revealed a fast inward current with an ionic sensitivity consistent with its being carried by Ca^{2+}. Like the

* Present address: Department of Pharmacological and Physiological Sciences, University of Chicago, Chicago, IL 60637, U.S.A.

K^+ current, the Ca^{2+} current was activated by small depolarizations from the resting potential, and over this voltage range it was about five to ten times smaller than the K^+ current. Its activation was more rapid than the fastest outward currents in high-frequency cells.

8. The inward current could also be carried by Ba^{2+}, which when substituted for external Ca^{2+} blocked the K^+ current. Measurements on cells with resonant frequencies of 13–240 Hz indicated that the peak Ba^{2+} current increased systematically with resonant frequency.

9. Manipulations such as external addition of Cd^{2+} which would be expected to reduce or abolish the Ca^{2+} current also blocked the K^+ current, consistent with a previous suggestion (Lewis & Hudspeth, 1983*b*) that the hair-cell K^+ conductance is gated by changes in intracellular Ca^{2+}.

10. Small steady depolarizations caused a pronounced increase in current fluctuations. The spectral density of the fluctuations in a given cell could be well fitted by the sum of two Lorentzians with half-power frequencies differing by an order of magnitude.

11. Both half-power frequencies changed with the resonant frequency of the hair cell, and the lower half-power frequency was consistent with that predicted from the time constant of the current relaxation. The variance-to-mean ratio for the fluctuations was about 1 pA in all cells. It is suggested the the fluctuations are dominated by the opening and closing of the K^+ channels, and that the intrinsic kinetics of these channels differ in cells with different resonant frequencies.

12. Single K^+ channels recorded in the cell-attached mode could be opened by depolarizations of the membrane under the patch electrode. At the start and end of a depolarizing step, the probability of channel opening rose and fell with an exponential time course, the time constant varying from 2 to 20 ms in different cells.

13. The results support the following conclusions: (i) the resonance behaviour and tuning of turtle cochlear hair cells are governed by the interplay of membrane Ca^{2+} and K^+ conductances; (ii) the resonant frequency is determined by the characteristics of the K^+ conductance, an increase in frequency being achieved largely by faster kinetics, but also to some extent by an increase in the size of this conductance; (iii) the magnitude of the Ca^{2+} conductance increases with resonant frequency and this may be needed to enhance the sharpness of tuning; (iv) the membrane properties are graded monotonically with distance along the basilar papilla.

INTRODUCTION

The receptor potentials of hair cells in the turtle cochlea are shaped not only by the characteristics of the input and transduction process, but also by a resonance within each cell that causes it to be maximally sensitive over a narrow frequency band (Crawford & Fettiplace, 1981*a*, *b*). This resonance, which has been demonstrated in other lower-vertebrate hair cells (Lewis & Hudspeth, 1983*a*; Ashmore, 1983; Ashmore & Pitchford, 1985; Fuchs & Mann, 1986), can be revealed as a damped oscillation in membrane potential evoked by an extrinsic current step. In the turtle, different hair cells respond preferentially to different frequencies, so that the cochlear epithelium is composed of an array of resonators, arranged tonotopically, that en-

compasses the animal's audible range from about 30 to 700 Hz (Crawford & Fettiplace, 1980). An important question is what factors change with position along the epithelium to produce the distribution of resonant frequencies.

It was originally proposed (Crawford & Fettiplace, 1981*a*) that the resonance was a consequence of time- and voltage-dependent conductances in the hair-cell membrane, and that specifically a voltage-sensitive K^+ conductance could confer on the hair cell the necessary inductive properties (Detwiler, Hodgkin & McNaughton, 1980), which when coupled with the membrane capacitance would generate resonance. Subsequently, the membrane currents of isolated hair cells were examined under voltage clamp (Lewis & Hudspeth, 1983*b*; Ohmori, 1984), and two major currents activated close to the resting potential were described: an inward current thought to be carried by Ca^{2+}, and an outward current believed to be a Ca^{2+}-activated K^+ current (Lewis & Hudspeth, 1983*b*; Ohmori, 1984). That these two currents, along with a membrane capacitance, would be sufficient to account for the hair-cell resonance has been established by reconstructing the oscillatory responses to current pulses (Lewis, 1985). This was done for a single resonant frequency by devising a kinetic scheme to describe the behaviour of the two currents under voltage clamp, and then using this scheme to predict the voltage changes to current steps. It is worth noting that the combination of a Ca^{2+} and a Ca^{2+}-activated K^+ conductance is also thought to underlie the very low-frequency oscillatory behaviour of some invertebrate neurones (e.g. Gorman, Hermann & Thomas, 1982).

The primary goal of the present work was to define the conductances responsible for resonance in turtle hair cells and ascertain how these conductances varied with the frequency to which the cells were maximally sensitive. Possible variables include the size and kinetics of the respective conductances, the speed of Ca^{2+} buffering within the cytoplasm (which could in turn limit the kinetics of activation of the K^+ conductance), or the cellular dimensions. The turtle cochlea is particularly suitable for such experiments since cells of a given resonant frequency can be selected according to their position along the basilar papilla (Crawford & Fettiplace, 1980). Cells could therefore be isolated from different regions, and by using patch-electrode techniques (Hamill, Marty, Neher, Sakmann & Sigworth, 1981), it was possible to measure membrane currents in cells with a broad range of resonant frequencies. The main conclusion from these experiments is that while several factors change, the most important one appears to be the speed of the K^+ conductance which varies over two orders of magnitude and may thus be the major determinant of resonant frequency. Preliminary accounts of some of the results have already been published (Art, Crawford & Fettiplace, 1986*a*,*b*).

METHODS

Preparation

Experiments were performed on hair cells isolated from the cochlea of the turtle *Pseudemys scripta elegans* (carapace lengths 80–120 mm). The cochlear duct and lagena were dissected out and bathed in an artificial perilymph (Table 1) containing the peptidase subtilisin BPN′ (Sigma, 30 μg/ml), and the cochlea opened and pinned to the bottom of a dissociation chamber. After 20 min, the tectorial membrane was peeled from the underlying epithelium. Hair cells were isolated enzymatically using a procedure developed in collaboration with Paul Fuchs which was similar to that previously applied to frog saccular hair cells (Lewis & Hudspeth, 1983*b*). The basilar papilla was

superfused with a low-Ca^{2+} (0·1 mM) perilymph to which had been added 0·5 mg papain/ml (Calbiochem), 0·1 mg bovine serum albumin/ml (BSA, Sigma) and L-cysteine to yield a concentration of 2·5 mM. During enzymatic digestion, the epithelium was loosened by undercutting successive supporting cells with a sharpened tungsten wire. After 25–30 min exposure, the papain-rich medium was replaced by several changes of low-Ca^{2+} solution containing 0·2 mg BSA/ml, which after a further 10–15 min was exchanged for a solution of normal ionic composition with the same BSA concentration.

The papilla was then divided transversely into quarters (see Fig. 2), and the cells harvested from each region a few rows at a time by gentle aspiration into a pipette whose opening had been fire polished to an internal diameter of 100–250 μm. The cells were plated into normal perilymph in one of four glass recording chambers. Both the cover-slips which formed the bottom of these chambers, and the transfer pipettes had been pre-treated with tri-*N*-butyl-chlorosilane (Pfaltz & Bauer) to prevent cell adhesion. Cells were subsequently allowed to settle for up to 45 min before recording commenced. In some later experiments, cells were pooled into fewer than four recording dishes. All experiments were performed on the stage of a Zeiss IM-35 inverted microscope equipped with Nomarski differential interference contrast optics (total magnification, 1000 ×) at room temperature (21–26 °C).

Hair cell morphology

The best recordings were from cells the ciliary bundles of which were intact and perpendicular to the apical surface of the cuticular plate. Such cells retained their morphology for 4 h after isolation, an example being shown in Pl. 1. The majority of cells examined were from the central region of the basilar papilla, the portion supported by the flexible basilar membrane. Difficulties associated with dissecting and isolating cells on the limbus in the hook region (see Miller, 1978, and diagram of cochlea in Fig. 2), near the junction of the cochlear duct with the saccule, precluded a systematic study of this most basal area.

A small variation in ciliary bundle height was observed with position along the basilar papilla, the length of the tallest row of stereocilia decreasing from about 9 μm at the apical end of the cochlear duct to 5 μm at the basal end. Such a variation has been noted previously in the cochleas of other vertebrates (Lim, 1980; Tilney & Saunders, 1983). In the present experiments, we could demonstrate a relationship to the resonant frequency of a hair cell so that cells with the longest bundles had the lowest resonant frequencies, and those with the shortest bundles the highest resonant frequencies. Although we cannot assign a functional significance to the variation in bundle height, it did serve as a useful index of both the expected frequency of a cell, and the region from which it had been isolated.

Recording instrumentation

When heat polished to an internal diameter of about 1 μm, soda-glass patch electrodes filled with standard internal K^+ solution (see Table 1) had resistances of 2–3 MΩ. For whole-cell recording in either current or voltage clamp (Hamill *et al.* 1981; Marty & Neher, 1983), the electrode was connected to a modified Yale MK V electrometer which had a 100 MΩ feed-back resistor in the head-stage, and a frequency boost circuit (Sigworth, 1983) to increase the band width of the current monitor to about 20 kHz. So as to allow ionic currents to be tape-recorded at maximum amplification, a circuit with a variable time constant and gain was driven by the voltage command to the head-stage, and used to create a signal that matched the capacitive transient at the start and end of a voltage-clamp step. This signal was not fed back to the input, but was subtracted from the total current at the output stage of the amplifier, thereby removing the large transient component. Both the difference signal and other data were stored on an FM tape recorder (band width 0–8 kHz) for subsequent analysis.

Experimental procedure

After sealing to the basolateral surface of a hair cell in voltage clamp, the electrometer was switched to current clamp, and continuity with the cell interior was attained following slight suction. The shunt resistance across the seal was normally between 1 and 10 GΩ. The value of the resting potential was stored on an internal sample-and-hold circuit, and so it was possible later to switch between current and voltage clamp and remain within 0·5 mV of the zero-current potential. The duration of recordings from most cells was typically 15 min.

The resonant frequency of a hair cell was first determined from the damped oscillatory voltage responses to small constant-current pulses (Fig. 1). In about a third of recordings, a steady depolarizing current of 10–50 pA was added to decrease the membrane potential to a value where the cell would display symmetric oscillations at the onset and offset of the superimposed pulse. The electrometer was then switched into voltage clamp, and by hyperpolarizing the cell by 25–30 mV to where all voltage-sensitive conductance were turned off, the current in response to a 5 mV step was used to adjust the compensation for the series resistance in the electrode and to nullify the capacity transient in the manner described above. The maintained response gave a measure of the leakage current. During later analysis, the net ionic current was obtained by subtracting from the raw averages a scaled version of this leakage current as well as any residual capacitive currents not removed by the nulling procedure.

Feed-back from the current monitor to the voltage command signal was used to compensate up

TABLE 1. Compositions of solutions (mM)

	External						
Solution	NaCl	KCl	$MgCl_2$	$CaCl_2$	$BaCl_2$	Tris Cl	TEA Cl
Normal	130	4	2·2	2·8	—	—	—
TEA	105	4	2·2	2·8	—	—	25
Ba^{2+}	130	4	—	—	5	—	—
Tris	—	4	2·2	2·8	—	130	—
K^+	—	134	2·2	2·8	—	—	—

	Internal			
	KCl	CsCl	$MgCl_2$	EGTA
K^+	125	—	2·8	5 (K^+ salt)
Cs^+	—	125	2·8	5 (Na^+ salt)

In addition to the salts listed, all external solutions contained D-glucose (8 mM) and HEPES (5 mM) neutralized with NaOH to pH 7·6; all internal solutions contained Na_2ATP (2·5 mM) and HEPES (5 mM) neutralized with KOH (K^+ solution) or NaOH (Cs^+ solution) to pH 7·2. In some experiments, BAPTA was substituted for EGTA in the internal solution. The internal solutions were used to fill the recording electrode during whole-cell recording. The high-K^+ external solution filled the electrodes for single-channel recording.

to 70% of the total series resistance; the remaining 1·5–5 MΩ resulted in average voltage-clamp time constants of about 35 μs. The value for the uncompensated series resistance inferred from the capacity transient (Marty & Neher, 1983) was used to correct the voltage-clamp potentials when constructing steady-state current–voltage relationships.

Repetitive voltage-clamp pulses were normally delivered at 10/s, though the rate was often slowed to 1/s to examine the Ca^{2+} current. Fatigue of the Ca^{2+} current was sometimes noted, and although we did not examine this in detail, it may be related to properties reported for some other preparations, where inactivation of the Ca^{2+} current is thought to result from accumulation of intracellular Ca^{2+} (Ashcroft & Stanfield, 1982; Eckert & Chad, 1984). The fatigue was not evident in the net currents recorded at 10/s.

Solutions

The compositions of external bath and internal pipette solutions are listed in Table 1. EGTA or occasionally BAPTA (1,2-bis(*o*-aminophenoxy)ethane-*N*,*N*,*N*′,*N*′-tetraacetic acid, BDH) was included in the internal solution to give a free Ca^{2+} concentration of less than 10^{-8} M, and Na_2ATP (Boehring–Mannheim) was added to try to maintain the Ca^{2+} current. In the final experiments, tetraethylammonium chloride (TEA) bought from Aldrich was used. TEA salts from Fluka, Fisons and Sigma were also tried but gave very small or variable Ca^{2+} currents, and furthermore two of these salts had a detectable amine smell. It has been suggested (Zucker, 1981) that this impurity can alter the intracellular Ca^{2+} buffering which might in turn affect the membrane conductance for Ca^{2+}.

All resting potentials have been corrected for the liquid junction potential measured between

normal perilymph and the K^+ intracellular solution, which made the real membrane potential 4 mV more negative than the observed value. Experiments with Cs^+-filled electrodes showed that the outward membrane current, as well as the voltage oscillations to extrinsic current pulses which were initially recorded on obtaining the whole-cell configuration, disappeared within 30 s, suggesting that the pipette solution quickly equilibrated with the cell interior.

Bath perfusion

For rapid exchange of the bathing solution in the vicinity of a particular cell, the perfusion method of Krishtal & Pidoplichko (1980) was employed. A U-shaped glass capillary 250 μm in diameter with a 200 μm diameter hole in its bottom wall was positioned within a few hundred micrometres of the cell under study. The influx and efflux of the tube were fed by a pair of peristaltic pumps, the relative rates of which were initially adjusted so as to draw solution from the bath into the tube. To superfuse a cell, the pump rates were electronically switched (Lamb, 1983), reducing the efflux and increasing the influx, and the test solution was expelled into the bath. Though this technique minimized exposure of other cells to the test solution, in each recording chamber only a single solution change was made when toxic chemicals such as Cd^{2+} or Ba^{2+} were applied.

Noise analysis

At each holding potential, current segments were low-pass filtered to prevent aliasing and digitized at 0·1–2 ms intervals. The mean level was substracted from each segment, and the resulting 1024-point array was multiplied by a cosine-taper window (Bendat & Piersol, 1971, p. 325), and transformed using an integer fast Fourier transform; the single-sided power spectrum (G_k) was computed from

$$G_k = \frac{2}{0{\cdot}875}\frac{h}{N}|X_k|^2,$$

where $k = 0, 1, 2 \ldots N-1$ and values of X_k are the Fourier coefficients at the discrete frequency values k/Nh with h the sample interval and N the number of data points. For each membrane potential, between 20 and 115 raw spectra were averaged. The spectrum due to the membrane current fluctuations was obtained by subtracting point-by-point the spectrum of the instrumentation noise, which was estimated from the residual noise present at a holding potential of about -80 mV, where all voltage-sensitive conductances would be turned off.

Single-channel currents

Single-channel currents were measured in the cell-attached mode (Hamill *et al.* 1981) using a List EPC-7 electrometer with 10 kHz output filtering. Electrodes coated with Sylgard were polished to 0·5 μm internal diameter, and when filled with a high-K^+ solution (Table 1) had resistances of 5–10 MΩ. Channel slope conductances were computed from stretches of data collected with maintained depolarizations and hyperpolarizations. Ensemble estimates of the non-stationary probability of channel opening during a voltage step were computed as described by Aldrich & Yellen (1983). For each sweep, all detectable opening and closing transitions were found and used to generate a schematic record that had a value of 0 when the channel was closed and 1 when it was open, and these idealized records were then averaged.

RESULTS

Resonant properties of isolated hair cells

The majority of solitary hair cells displayed properties akin to those of cells in the intact papilla, and in particular produced damped oscillations in membrane potential at the onset and termination of an imposed current step. Examples of this resonant behaviour can be seen in Fig. 1, which gives the oscillatory voltage responses of five cells from different regions of the papilla. The frequency of the oscillations is given beside each averaged record and it is clear that a range of resonant frequencies was obtainable. In the absence of deliberate stimulation, the membrane potential of an isolated cell oscillated spontaneously at its resonant frequency, a phenomenon which

has been described earlier from intracellular recordings in the whole cochlea (Crawford & Fettiplace, 1980). Occasionally, in low-frequency cells, this spontaneous activity would erupt into slow action potentials with an amplitude of 40 mV or more.

The parameters of the resonance, its resonant frequency and quality factor, were dependent on membrane potential, as for cells of the intact organ (Crawford &

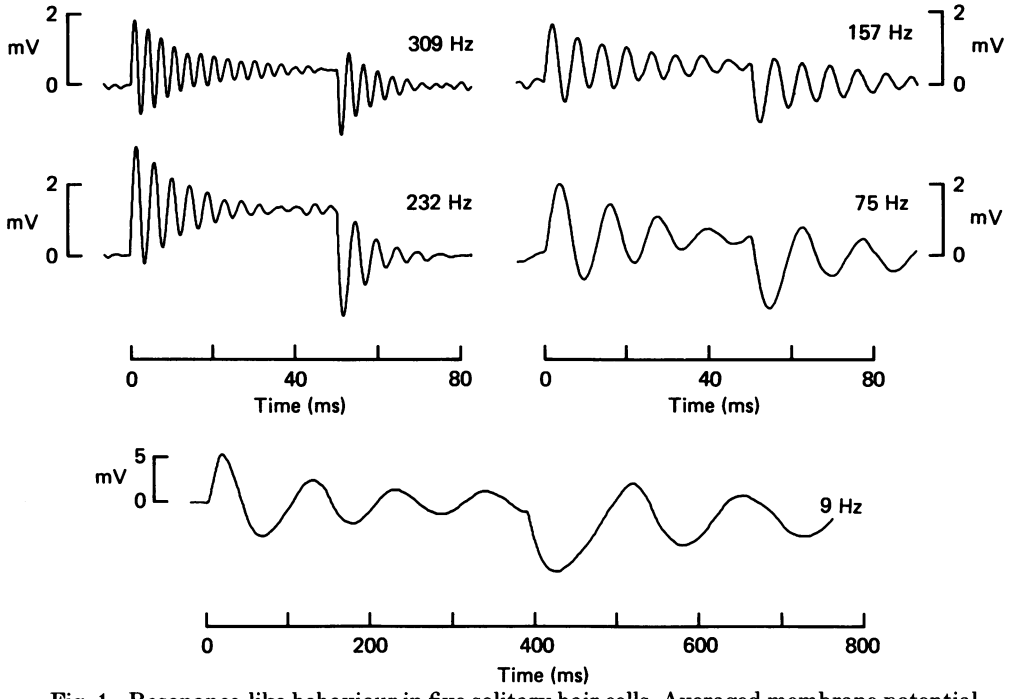

Fig. 1. Resonance-like behaviour in five solitary hair cells. Averaged membrane potential changes are shown in response to rectangular depolarizing current pulses that began at time zero and had a duration of 50 ms for all but the bottom record where it was 395 ms. Resonant frequency (f_0), determined from the frequency of the damped oscillations, is given beside each trace. Quality factor (Q) of resonance calculated from $Q = [(\pi f_0 \tau_0)^2 + 1/4]^{1/2}$ where τ_0 is the time constant of decay of the oscillations at the current onset. Ordinates are relative to the resting potential. f_0, Q, resting potential and current magnitude were: 309 Hz, 14, −49 mV, 50 pA; 232 Hz, 9·5, −51 mV, 50 pA; 157 Hz, 12, −50 mV, 20 pA; 75 Hz, 8, −51 mV, 10 pA; 9 Hz, 6, −54 mV, 6 pA.

Fettiplace, 1981*a*; Art, Crawford, Fettiplace & Fuchs, 1985) and so it was necessary to adopt a criterion to define properly the optimum frequency of a given cell. The quality factor deduced from the frequency of the oscillations to extrinsic currents and the time constant of their decay (Crawford & Fettiplace, 1981*a*), has been found to be a bell-shaped function of membrane potential. A particularly striking example of this was shown in Art *et al.* (1985), and a qualitatively similar relationship was demonstrable in the isolated cells, with the quality factor having a maximum value at or a few millivolts positive to the resting potential. A cell's resonant frequency was therefore taken as that frequency at which the quality value was maximal. Defined in this way it varied from 9 to 350 Hz, and values for the quality factors

of most cells lay between 5 and 31 (see legend to Fig. 1). Their resting potentials ranged from -41 to -61 mV (mean $\pm$ S.D., -51 ± 4 mV; $n = 35$).

A proportion of the cells were significantly hyperpolarized at rest with respect to the membrane potential for peak quality factor. This was regarded as an abnormal

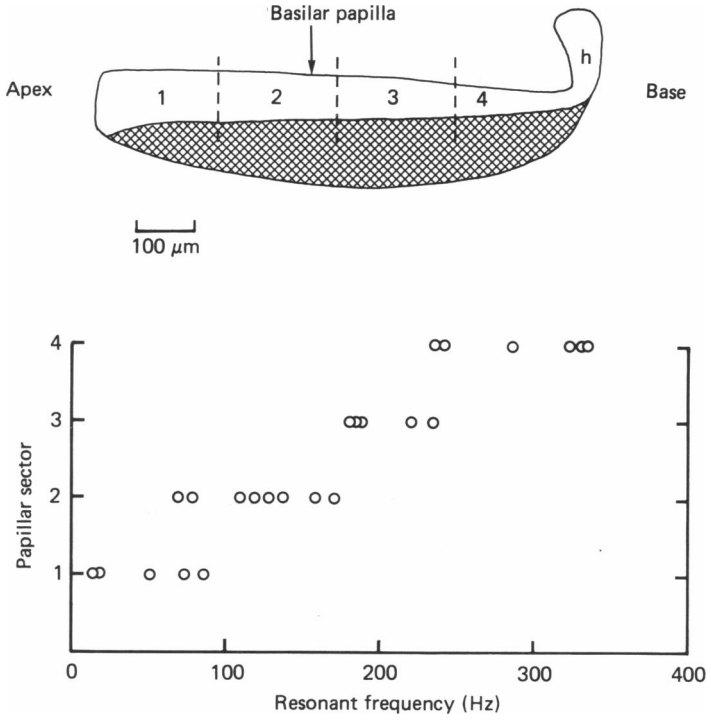

Fig. 2. Variation of resonant frequency with location of hair cell on the basilar papilla. The upper sketch shows the turtle cochlea with the cross-hatched area indicating the free basilar membrane. Hair cells were collected from each of four sectors of the papilla excluding the hook region (h; see Methods). Lower graph gives the resonant frequencies of cells isolated from the different sectors. Results are pooled from a number of animals.

condition, both because it had not been observed in hair cells in the intact papilla, and because it became more prevalent in the later stages of an experiment, suggesting some degenerative change. If a cell was only a few millivolts hyperpolarized, then a standing depolarizing current of up to 50 pA was injected to push the cell into the region where its tuning was greatest, and where a superimposed small current step would generate approximately symmetrical voltage oscillations at the start and end of the pulse. The new membrane potential was taken as the holding potential for later voltage-clamp measurements. Cells that were well out of the voltage range for maximal tuning were excluded from the subsequent analysis. One possible explanation for this abnormal behaviour might be a progressive loss of the transducer conductance, which from separate experiments (Art, Crawford & Fettiplace, 1986*b*) was known to be present in the isolated cells. Since this conductance is thought to be partially turned on at rest (Crawford & Fettiplace, 1981*b*), it would contribute

a standing inward current, and loss of the transducer would thus result in a hyperpolarization of the cell from its normal resting potential.

Tonotopic organization

Previous studies (Crawford & Fettiplace, 1980; Art *et al.* 1986*a*) have shown that the hair cells are arranged tonotopically in the turtle cochlea with the frequency of maximal sensitivity increasing roughly exponentially with distance from the lagenar end of the cochlear duct. To examine whether the resonant frequencies of isolated cells matched their expected values in the intact cochlea, that portion of the papilla excluding the most basal hook region (see Fig. 2) was divided into four sectors of equal length, and cells were harvested from each sector into a separate experimental dish. The distribution of resonant frequencies for each of the four dishes is shown in Fig. 2, the sectors being numbered sequentially from the lagenar end. It is evident that the dishes contained subsets of the frequency population, and the orientation of the map was correct with the lowest frequencies emanating from the papillar sector adjacent to the lagena and the highest frequencies from that closest to the saccule. To obtain a quantitative assessment of the distribution of resonant frequencies in the isolated cells, the frequencies at the transition from one sector to the next were compared with those frequencies expected at the appropriate distances along the cochlea, i.e. at a quarter, a half and three-quarters of its length. From the data in Fig. 2, transition frequencies of about 75, 175 and 235 Hz were inferred as compared to 55, 140 and 290 Hz expected from the tonotopic organization in isolated papillar measurements (Art *et al.* 1986*a*); the latter had been made under comparable ionic conditions in cochleas of about the same size. The agreement between the two sets of numbers is reasonable considering the difficulty of reproducibly partitioning the papilla during each dissociation, and therefore we have no reason to believe that the frequency distribution observed in isolated cells is greatly different from that in the intact epithelium.

Net currents and current–voltage relationships of isolated cells

The standard procedure for an experiment was initially to determine the resonant frequency of a cell and then switch to voltage clamp to measure the underlying currents; the holding potential was normally the resting potential. Average membrane currents to a series of voltage-clamp steps are shown in Fig. 3, along with the oscillatory response to a current pulse recorded in the same cell. The records show that with positive voltage steps, a maintained outward current developed, and its magnitude grew dramatically with increasing depolarization, reflecting a strong outward rectification as reported previously (Corey & Hudspeth, 1979; Art *et al.* 1985). Comparable hyperpolarizations elicited a more limited inward current.

The rectification is evident in the steady-state current–voltage relationship, which is plotted as the squares in Fig. 4*A*, along with measurements from three other cells with a range of resonant frequencies. In each case, the clamp potentials have been corrected for the uncompensated series resistance in the electrode. The shape of the current–voltage relationship was found to be similar in all cells, being flat at hyperpolarized levels and increasing its slope with depolarization through the resting potential. As will be established later, the net current was carried mainly by K^+, and

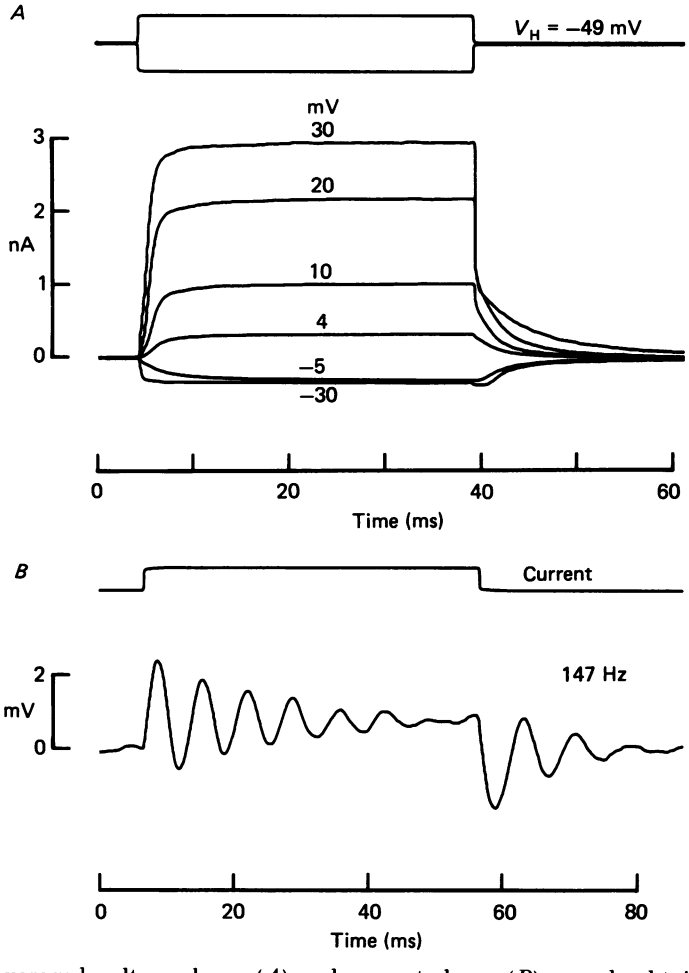

Fig. 3. Averaged voltage-clamp (*A*) and current-clamp (*B*) records obtained from the same hair cell. *A*, net currents elicited in response to voltage steps delivered from a holding potential (V_H) equal to the resting potential (−49 mV); leakage and capacity currents have been subtracted, and outward ionic currents are denoted as positive. Command voltages relative to the holding potential are given in mV next to the traces and have not been corrected for the residual series resistance in the electrode (3·3 MΩ). *B*, changes in membrane potential produced by 20 pA depolarizing current pulses, current monitor shown above. The cell's resonant frequency was 147 Hz, estimated from the frequency of the oscillations during the current. This record was obtained prior to the voltage-clamp run.

therefore the form of the current–voltage curve may be largely dominated by a K^+ conductance, gated directly or indirectly by membrane potential, that is turned off by hyperpolarization and turned on further by depolarization from the resting potential. This conductance would thus be partially activated at the membrane potential where the resonance behaviour is most prominent in current clamp.

While the range of membrane potentials over which the conductance was activated was comparable in all cells, the size of the current scaled with the resonant frequency

of the cell. This can be seen in Fig. 4*A*, where the sets of points for the four cells diverge from the origin, and at all potentials the current increases monotonically with frequency. The ranking is also evident in Fig. 4*B*, which provides a plot of the steady-state input conductances in twenty-six cells as a function of their resonant

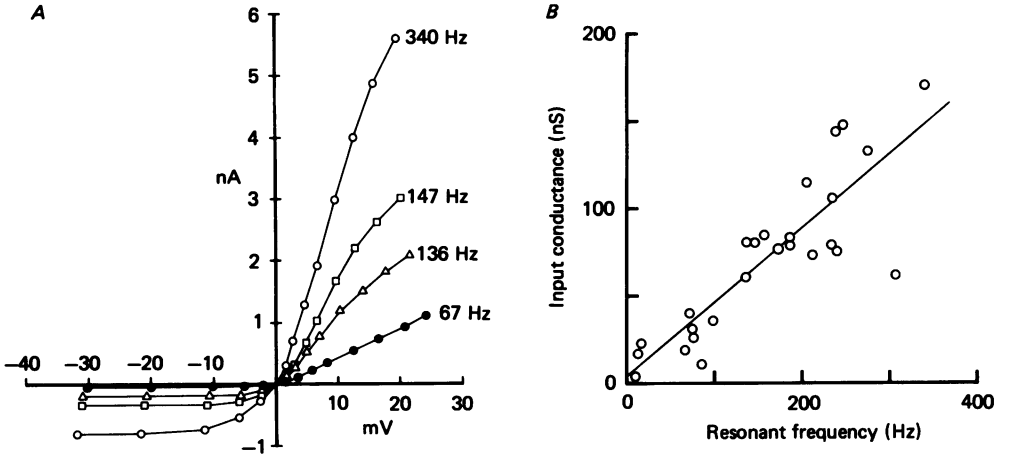

Fig. 4. *A*, steady-state current–voltage relationships in four different hair cells, the resonant frequencies of which are given next to the plots. Outward current produced by depolarization is denoted as positive. All potentials have been corrected for the residual series resistance in the electrode as described in the Methods, and are plotted relative to the holding potentials, which were: 340 Hz, −42 mV; 147 Hz, −49 mV; 136 Hz, −46 mV; 67 Hz, −51 mV. Note that at each potential, the current magnitude increases with the resonant frequency of the cell. *B*, plot of steady-state slope conductance at the resting potential as a function of resonant frequency in twenty-six cells. Straight line is a least-squares fit with a regression coefficient of 0·86.

frequency: despite the scatter, the input conductance on average increased with frequency, the straight line being the least-squares fit to the points. The simplest conclusion is that cells of a higher resonant frequency have a larger membrane conductance, and this arises not because they sit at different places on their respective current–voltage curves, but more probably because their membranes contain a greater number of conducting channels.

Kinetics of the net current

This section describes the variation with resonant frequency in the time course of the net current evoked by a small voltage-clamp step. The time course was to within experimental error invariant with the amplitude of the step up to about 5 mV of depolarization and, over this range, the kinetics were unlikely to be distorted by any uncompensated series resistance in the electrode. Examples of net currents produced by 2 or 4 mV depolarizing steps are shown in Fig. 5 for four cells of various frequencies, and leakage and capacitance currents have been subtracted from each average trace. Irrespective of frequency, the essential features of the kinetics were similar: the current developed after a small delay at the beginning of the step, and at its end declined approximately exponentially. Inspection of the records in Fig. 5

reveals that both onset and decay of the current were slower in cells of a lower resonant frequency.

To quantify the kinetics, the time course of the decline of the current on repolarization was measured, and the major component of the decay was found to

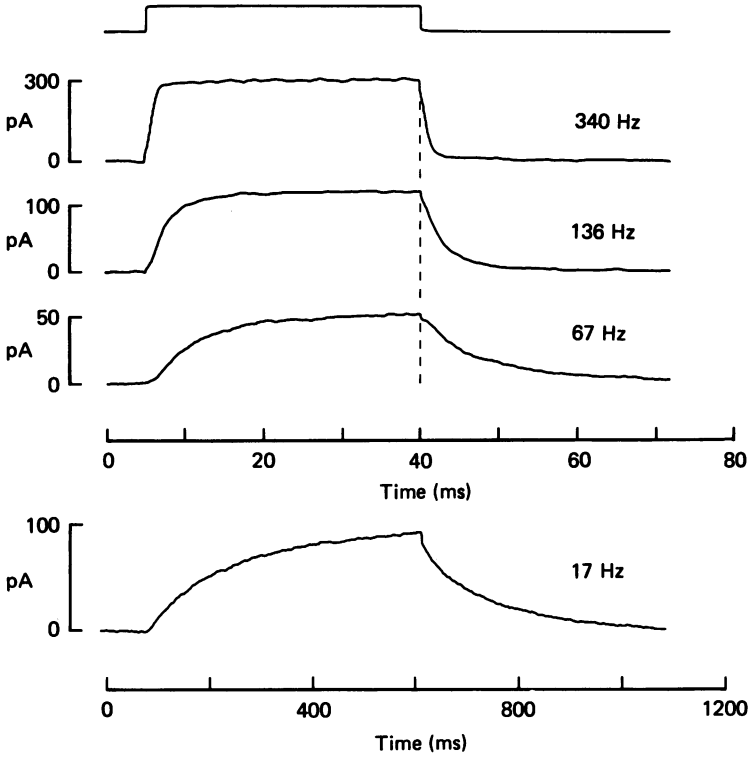

Fig. 5. Kinetics of membrane currents for small positive voltage steps in four cells of different resonant frequencies (shown beside traces). Timing of voltage pulse is shown above, and its magnitude was 2 mV for the top three traces and 4 mV for the bottom trace. Each record is the average of fifty presentations and leakage and capacity currents have been subtracted. Current–voltage relationships shown for three of the cells in Fig. 4*A*. Holding potentials and cell capacitances were (from the top down): −42 mV, 15·5 pF; −46 mV, 12·1 pF; −51 mV, 11·3 pF; −46 mV, 9·9 pF. Note that the speed of the onset and decay of the current increased with the resonant frequency, the bottom trace being shown on a slower time-scale than the others. Temperature, 24–26 °C.

be characterized by a single time constant. For the cells illustrated, the time constant decreased inversely with resonant frequency, from 138 ms in the 17 Hz cell to 0·8 ms in the 300 Hz cell. The relaxation time constants for a number of cells are collected in Fig. 6, from which it is evident that the time constant varied systematically with frequency. The tightness of the relationship between the two would be consistent with the kinetics being a major factor in determining the resonant frequency of a hair cell. Although the current onset had a more complex and sigmoidal time course, it showed a similar systematic variation with resonant frequency.

It is well established (Mauro, Conti, Dodge & Schor, 1970; Detwiler *et al.* 1980) that a membrane that undergoes voltage-dependent conductance changes can, under some conditions, behave as though it contained an inductance. The presence in the hair

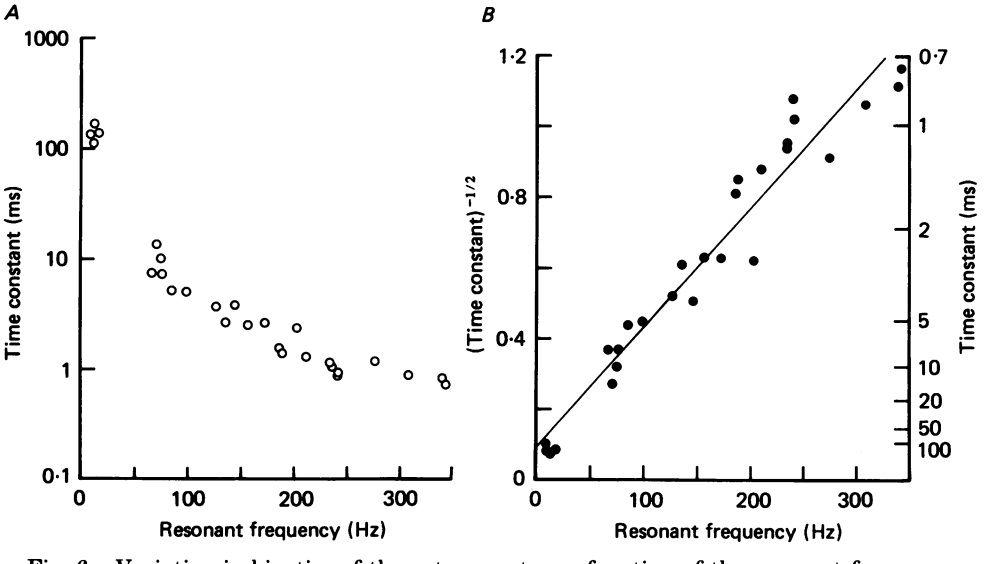

Fig. 6. Variation in kinetics of the net current as a function of the resonant frequency of the hair cell. *A*, principal time constant of the tail-current decay following a small depolarizing voltage step is plotted against resonant frequency for twenty-seven cells. *B*, same measurements with left-hand ordinate corresponding to the reciprocal of the square root of the time constant in milliseconds, which increases approximately in proportion to the resonant frequency. Straight line is a least-squares fit with a regression coefficient of 0·97.

cell of an equivalent inductance is essential to generate the resonant behaviour which has previously been modelled by an electrical circuit comprising a capacitance in parallel with the series combination of the inductance and a resistance (Crawford & Fettiplace, 1981*a*). The resonant frequency (f_0) of this circuit is determined solely by the inductance (L) and capacitance (C):

$$f_0^2 = \frac{1}{4\pi^2 LC}. \tag{1}$$

For a simple voltage-sensitive conductance the activation of which is controlled by a first-order rate process of time constant τ, the equivalent inductance for small perturbations in membrane potential is given by (Detwiler *et al.* 1980; Ashmore & Attwell, 1985):

$$L = \frac{\tau}{\frac{\partial g}{\partial V}(V - V_R)}, \tag{2}$$

where g is the conductance, V the membrane potential and V_R the equilibrium potential of the ionic species conveying the current. If the conductance is activated by depolarization, as is usually the case, the membrane will behave inductively only

when the membrane potential is positive to the equilibrium potential. Thus during a small depolarization, the current flowing through the voltage-sensitive channels initially increases with time and opposes the change in membrane potential. Combining eqns. (1) and (2) gives the relationship between the frequency of resonance and the time constant with which the current is activated in voltage clamp:

$$f_0^2 = \frac{\frac{\partial g}{\partial V}(V - V_R)}{4\pi^2 C\tau}. \quad (3)$$

In the absence of variations in parameters other than the time constant, the resonant frequency should be proportional to the reciprocal of the square root of the time constant ($\tau^{-\frac{1}{2}}$). That this is approximately the case can be seen in Fig. 6*B*, where the results of Fig. 6*A* have been replotted with the reciprocal of the square root of the time constant on the ordinate.

Although implying that a variation in the time constant may be sufficient to account for the entire range of resonant frequencies, the analysis is clearly over-simplified. From the sigmoidal nature of the current onsets, the gating of the conductance cannot be completely described by first-order kinetics. Furthermore, the magnitude of this conductance exhibited some frequency dependence (see Fig. 4) although less pronounced than that of the time constant. However, the cell's membrane capacitance, which may largely determine the capacitance in the equivalent circuit, showed no systematic trend with resonant frequency. For the cells of Fig. 6, it ranged from 9·9 to 15·5 pF (mean ± S.D., 12·1 ± 1·7 pF; $n = 26$).

Tail currents

This section describes measurements of the tail currents at different membrane potentials, providing direct information about the voltage dependence of the major conductance which we will show is due to K^+. In Fig. 7 are plotted for four different cells the amplitudes of the tail currents. These were derived by extrapolating the exponential current relaxation back to the break of the pulse. The measurements were made on families of voltage-clamp records similar to those illustrated in Fig. 3, and are all for repolarizations to the resting potential. The currents are outward and are expressed as the difference between the tail current at a given membrane potential and the tail current obtained with a 30 mV hyperpolarization, at which potential the voltage-sensitive conductance would be completely turned off. The tail current, which should be proportional to the fraction of channels activated at each membrane potential, had a similar voltage dependence in all cells, increased approximately exponentially around the resting potential and saturated at depolarized levels. As can be seen in Fig. 7, the saturated current increased systematically from 480 to 3700 pA with the cell's resonant frequency, which is consistent with the notion that higher-frequency cells had a larger conductance. From the limiting slopes at negative potentials, we estimated that the current initially grew e-fold in 2·5 to 4·0 mV. The steep voltage dependence was a ubiquitous finding (mean ± S.D., 3·2 ± 0·6 mV; $n = 17$) and has been predicted by earlier micro-electrode measurements (Art *et al.* 1985).

When the hair cell was repolarized to different potentials at the end of a positive voltage step, the current relaxation, which still followed an exponential time course,

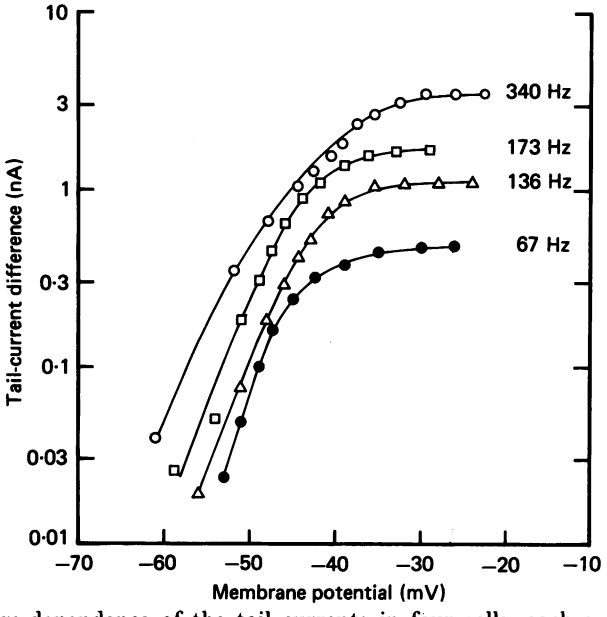

Fig. 7. Voltage-dependence of the tail currents in four cells, each symbol denoting a different cell with its resonant frequency given beside the plot. Positive and negative voltage steps were presented from a holding potential set to the resting potential and the initial amplitude of the tail current on repolarization is plotted against the membrane potential during the step. The ordinate is the difference between the tail current at a given membrane potential and the tail current obtained with a 30 mV hyperpolarization. Note that the saturating current increases with resonant frequency. Continuous lines drawn through points by eye. Resting potentials of cells; ○, −42 mV; □, −49 mV; △, −46 mV; ●, −51 mV.

was found to speed up with hyperpolarization (Fig. 8*A*). Collected measurements on four cells are presented in Fig. 8*B*, where the time constant of the tail current is plotted logarithmically against membrane potential. The results show that the time constant shortened e-fold in about 24 mV of hyperpolarization. Experiments in which the repolarization potential was altered were also performed to determine the reversal potential of the tail current. The clearest reversals were achieved in low-frequency cells, and records from one such cell are illustrated in Fig. 8*A*. There the tail current changed polarity between −78 and −88 mV, and a reversal potential of −82 mV was interpolated. In cells of higher resonant frequencies, the instantaneous current–voltage relationship was very non-linear at negative potentials and reversed (inward) currents were more difficult to measure. Nevertheless we obtained several estimates of the reversal potential which had a mean value of -82 ± 2 mV in six cells with resonant frequencies from 9 to 211 Hz. The value of the reversal potential indicates that the outward current is predominantly due to K^+, and, assuming a constant field relationship, the permeability ratio for K^+ over Na^+ is calculated to be about 80, when the intracellular concentrations of these ions are taken to be those of the solution in the recording electrode.

In some cells, an additional current was turned on at membrane potentials negative to −90 mV, and had a similar voltage dependence to the inward rectifier current

reported previously in chick hair cells (Ohmori, 1984). Since this current was not activated near the resting potential, it was not characterized further.

Confirmation of the major role of K^+ was provided by the observation that the outward current was absent when Cs^+ was substituted for K^+ in the intracellular solution that filled the patch electrodes. Loss of the outward current revealed a small

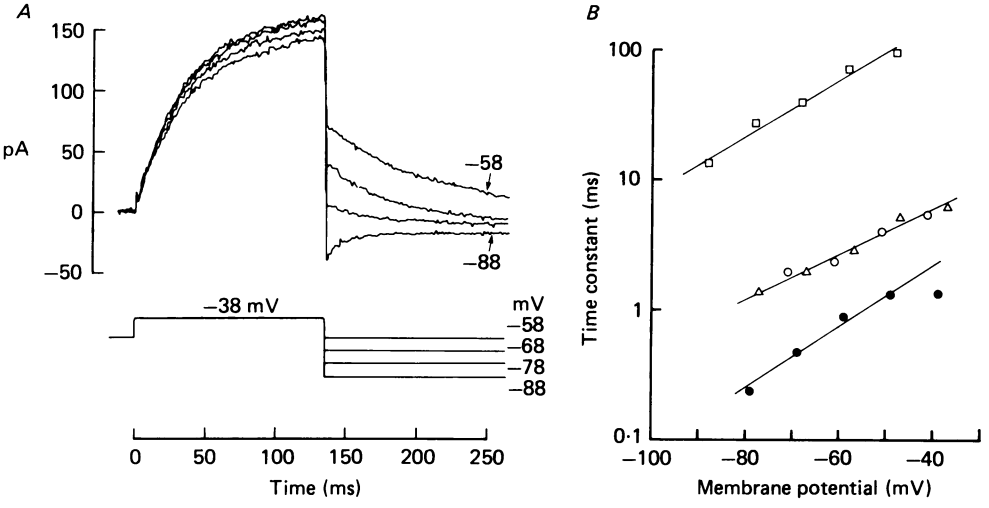

Fig. 8. *A*, tail-current reversal in a hair cell of low resonant frequency (9 Hz). Superimposed current records are shown above with the corresponding voltage commands below. Note that the tail current decayed faster as the cell was repolarized to more negative potentials, and that its polarity was reversed by −88 mV. *B*, voltage dependence of the time constant of decay of the tail currents in four different cells. A net outward current was activated by a 20 mV depolarization from the resting potential, and the tail currents were elicited by repolarization to different levels as in *A*. Straight lines were drawn by eye through the points and correspond to e-fold changes of time constant in 20, 24 and 28 mV respectively from the top. Resonant frequencies of cells: □, 9 Hz; ○, 76 Hz; △, 76 Hz; ●, 211 Hz.

fast inward current (Fig. 11*A*), and an example of the steady-state current–voltage relation under such conditions is shown in Fig. 11*B*. As will be argued later, the inward current is thought to be a Ca^{2+} current which is described in detail in the next section. When Cs^+-filled electrodes were used, the cells were often depolarized in current clamp and showed none of their normal resonant properties. By contrast, replacement of external sodium by Tris, which permeates poorly through many cation-selective channels, left both the outward current and resonant behaviour intact.

Isolation of the Ca^{2+} current

This section describes the separation of the net membrane current into two components, believed to be carried by K^+ and Ca^{2+} respectively, as has been reported previously in other types of hair cell (Lewis & Hudspeth, 1983*b*; Ohmori, 1984). The main goal of our experiments was to estimate the relative sizes of the two components, measured in the same cell. Secondly, we wished to determine the speed of the Ca^{2+}

current since this could conceivably limit the time course of the K^+ current if the latter were activated by Ca^{2+} influx. The Ca^{2+} current was unmasked on blocking the K^+ conductance by external application of 25 mM-TEA.

Average records showing the currents with and without TEA for a series of voltage-clamp steps from the resting potential are presented in Fig. 9*A*. The control

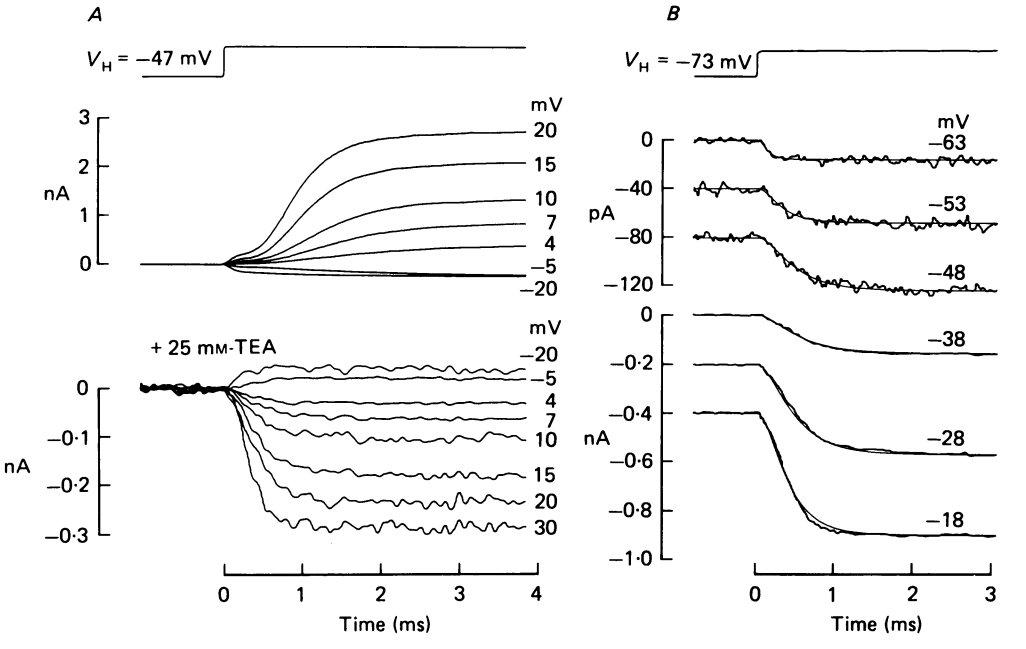

Fig. 9. Average membrane currents before (above) and during (below) external perfusion with 25 mM-TEA. For each family, the cell was held at −47 mV and stepped to various levels, the *change* in potential being indicated in mV beside each trace. Leakage and capacity currents have been subtracted, and the timing of the voltage step is shown above. Note that the net outward current evoked by depolarization for the control became inward in the presence of TEA. Five to fifty presentations were averaged for controls and two to five with TEA. The initial hump in the control records represents the instantaneous component, the onset of which is smoothed due to filtering by the recording system. *B*, same cell as in *A*; membrane currents from a holding potential of −73 mV during superfusion with TEA; absolute membrane potentials during step given next to traces. The current levels have been displaced vertically for display purposes but all had same starting value. The superimposed smooth curves were calculated from an m^2 relation (eqn. (4)) with τ_m = 0·08 ms (−63 mV); 0·22 ms (−53 mV); 0·34 ms (−48 mV); 0·38 ms (−38 mV); 0·34 ms (−28 mV); 0·28 ms (−18 mV). Resonant frequency of hair cell, 206 Hz. Temperature, 24 °C.

records (above) demonstrate the usual large outward current turned on by depolarization. However, in the presence of TEA (below), the current became inward for positive steps and outward for negative steps; thus the current was activated in the voltage range around the resting potential (−47 mV for the cell illustrated), and it increased with depolarization, attaining a maximum amplitude of 300 pA at about −20 mV. For further depolarization, its magnitude declined. This current was

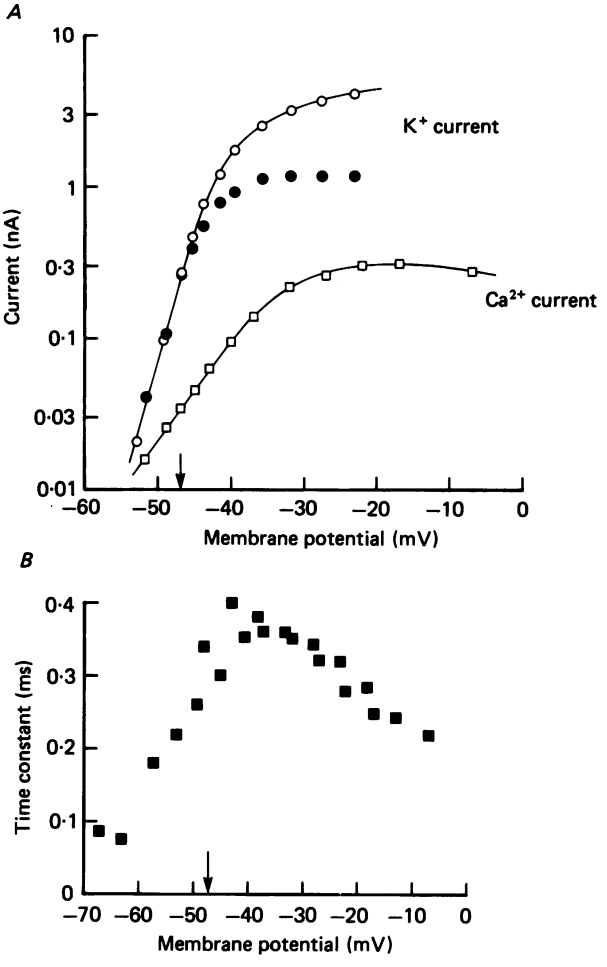

Fig. 10. *A*, current–voltage relationships for cell of Fig. 9: □, steady-state currents with 25 mM-external TEA; ○, differences between steady-state currents in the absence and presence of TEA. The current magnitudes were measured relative to the current level produced by a 30 mV hyperpolarization (○, outward; □, inward). The abscissa is the absolute membrane potential corrected for residual series resistance in the electrode (1·7 MΩ). Arrow indicates the holding potential (−47 mV). ●, initial amplitudes of the tail currents measured from control responses, also expressed relative to the value for a 30 mV hyperpolarization. The major conducting ion is thought to be K^+ (○, ●) and Ca^{2+} (□). Lines drawn by eye through points. *B*, voltage dependence of the time constant of activation of the Ca^{2+} current, derived from theoretical fits similar to those in Fig. 9*B*. Temperature, 24 °C.

identified as a Ca^{2+} current since, in other experiments, it was shown to be enhanced by replacement of external divalent cations by Ba^{2+} (Fig. 13*B*), and it could be abolished by removal of external Ca^{2+} (Fig. 11) or addition of 4 mM-Co^{2+}.

The peak size of the Ca^{2+} current was substantial considering the small dimensions of the hair cells, and it ranged from 140 to 700 pA (mean, 320 pA; 2·8 mM external Ca^{2+}) in seven experiments with TEA. The isolation of the current depended crucially

on the source of the TEA, and of several brands employed (see Methods) only one consistently gave Ca^{2+} currents, the values for this one source having been quoted. The chosen brand of TEA was effective in exposing the Ca^{2+} current in cells of all resonant frequencies apart from one very-low-frequency cell of 11 Hz where it caused only partial block of the K^+ current. However, in all these experiments, there was no obvious relationship between the Ca^{2+} current's size and the cell's resonant frequency, though any possible correlation might have been obscured by secondary effects of TEA. An alternative method to reveal a correlation is described later using Ba^{2+} to block the K^+ current.

The steady-state amplitudes of the Ca^{2+} and K^+ currents are plotted as the open symbols in Fig. 10*A*, values for the latter being obtained by subtracting the Ca^{2+} current from the net current in the absence of TEA; each measurement has been plotted with respect to the maintained current level evoked by a large (30 mV) hyperpolarizing step. Both currents were activated steeply by depolarization and, from the limiting slopes of the lines drawn through the points, we estimated that the K^+ current grew e-fold in 2·5 mV as compared to 6·7 mV for the Ca^{2+} current, the ratio of voltage sensitivities thus being nearly 3. The filled symbols are the amplitudes of the tail currents obtained from control responses as described earlier. The tail current, which is proportional to the K^+ conductance, saturated at a membrane potential where the Ca^{2+} current was still rising. Therefore, this saturation probably results when the K^+ channels attain their maximum probability of being open.

In contrast to the saturation of the tail current, the steady-state K^+ current continued to rise with depolarization. The reason for this can be seen by considering the dual effect of membrane potential on current flow. For a voltage-clamp step to a given membrane potential, V, the steady-state current reflects the number of channels open at V and the electromotive driving force $(V - V_K)$, where V_K is the K^+ equilibrium potential. If all the channels are open, the current will still increase with depolarization. The amplitude of the tail current however is related solely to the number of channels opened at V, since the measurements are made at a constant electromotive driving force equal to the difference between V_K and the holding potential.

At the resting potential, the amplitude ratio of the Ca^{2+} to K^+ currents was about 0·1 in the cell illustrated, and for other cells it ranged from 0·06 to 0·2. Considering the various experimental factors that might reduce the observed Ca^{2+} current, it seems likely that the larger value more closely approximates the true ratio. Nevertheless these ratios indicate that the Ca^{2+} current made only a minor contribution to the net current, measurements of which must almost entirely reflect the behaviour of the K^+ system.

One of the most striking features of the traces in Fig. 9 is the speed of onset of the Ca^{2+} current as compared to the net current, which rose only after a delay. To quantify the kinetics of the Ca^{2+} current (I_{Ca}), the onsets recorded from a holding potential of -73 mV (see Fig. 9*B*) were fitted with a function of the form:

$$I_{Ca}(t) = \bar{I}_{Ca}(1 - \exp(-t/\tau_m))^2, \quad (4)$$

where $\bar{I}_{Ca}$ is the steady-state Ca^{2+} current. This is the simplest scheme consistent with the sigmoidal nature of the current onset as found in other cells (e.g. Hagiwara &

Ohmori, 1982). Eqn. (4) provided a good description of the rising phase of the currents in Fig. 9*B*, and, as in other preparations (Hagiwara & Ohmori, 1982; Fenwick, Marty & Neher, 1982) the inferred time constant, τ_m, was found to be voltage dependent (Fig. 10*B*). Its value near the resting potential was close to 0·3 ms, and therefore an order of magnitude smaller than the time constant of relaxation of

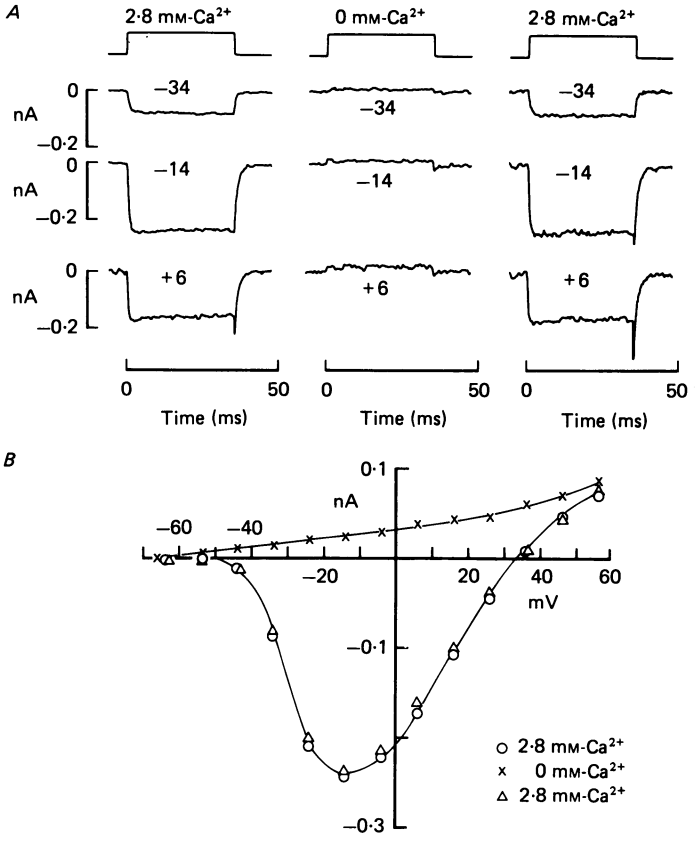

Fig. 11. Inward membrane currents recorded with a Cs^+-filled electrode. *A*, single examples of currents during voltage clamp to the potential indicated beside each trace, before, during and after removal of 2·8 mM extracellular Ca^{2+}. Capacitive currents have been subtracted. Holding potential, −74 mV. *B*, steady-state current–voltage relationships for the same cell in the presence (○, △) and absence (×) of 2·8 mM external Ca^{2+}. Measurements made on records similar to those in *A*, and the controls are before and after Ca^{2+} removal. Abscissa is absolute membrane potential.

the K^+ current, in this case 2·6 ms. Similar fast kinetics were observed in three other cells studied, also much faster than the relaxations of their respective K^+ currents.

Ba^{2+} currents

Owing to the somewhat variable effects of using TEA, we looked for an alternative method of judging the size of the inward current in cells of known resonant frequency, and found that replacement of external divalent cations by Ba^{2+} would both abolish

the K^+ current and unveil the inward current. Examples of this manoeuvre are shown in Fig. 12 for two cells of quite different resonant frequencies, the lower-frequency one being displayed on the left. In each case with Ba^{2+} substitution, the outward current was replaced by an inward current of comparable magnitude. Taking account

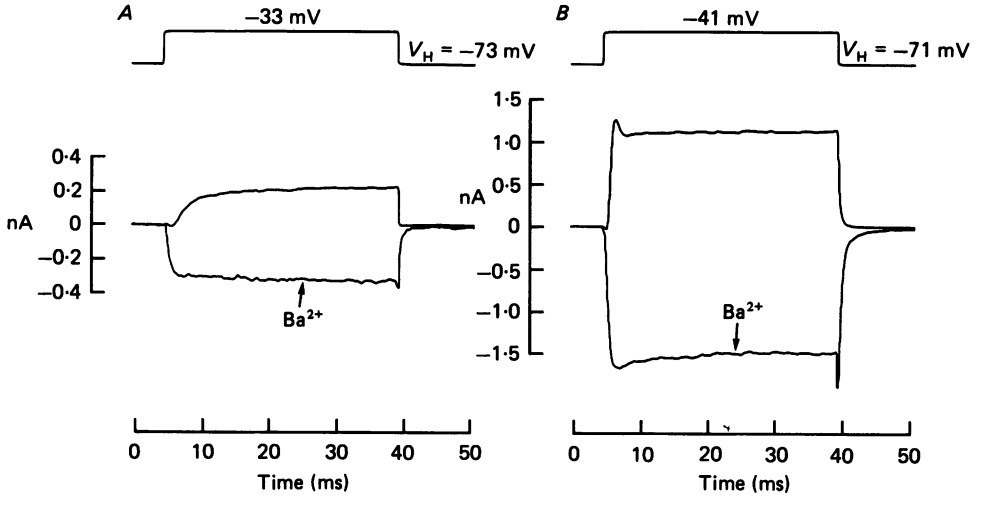

Fig. 12. Effects of replacing external divalent cations by 5 mM-Ba^{2+} in two hair cells. For each cell, the averaged currents with and without Ba^{2+} are shown for positive voltage steps from a holding potential hyperpolarized to the resting potential, the absolute membrane potentials being indicated on the voltage monitors above each pair of records; leakage and capacity currents have been subtracted. Resting potentials and resonant frequencies of cells were: −47 mV, 85 Hz (*A*); −59 mV, 240 Hz (*B*). Note that Ba^{2+} induced an inward current, and that both inward and outward currents were about five times larger in the higher frequency cell. The Ba^{2+} currents displayed are close to maximal in each case. The patch electrode was filled with normal (high-K^+) intracellular solution.

of the difference in scaling of the ordinates, it can be seen that both inward and outward currents were about five times larger in the higher-frequency (240 Hz) cell than in the lower-frequency (85 Hz) cell. For each of the experiments depicted the inward currents were close to maximal.

The steady-state current–voltage relationship in the presence of Ba^{2+} is shown for one of the cells in Fig. 13*A*, indicating that the inward current increased with depolarizations up to about −20 mV. The measurements on the other cell were less complete, but exhibited a qualitatively similar dependence on membrane potential. That Ba^{2+} was indeed traversing the Ca^{2+} channel could be demonstrated in recordings with Cs^+-filled electrodes. Current–voltage relationships under these conditions are presented in Fig. 13*B*, showing the effects of Ba^{2+} substitution along with the controls in normal external Ca^{2+} (2·8 mM) before and after Ba^{2+} substitution. In this experiment, as with those employing standard K^+-filled electrodes, both external divalent cations, Ca^{2+} and Mg^{2+}, were substituted to give a final Ba^{2+} concentration of 5 mM. From the sets of curves, it can be seen that the *peak* Ba^{2+} current was approximately three times that for Ca^{2+}.

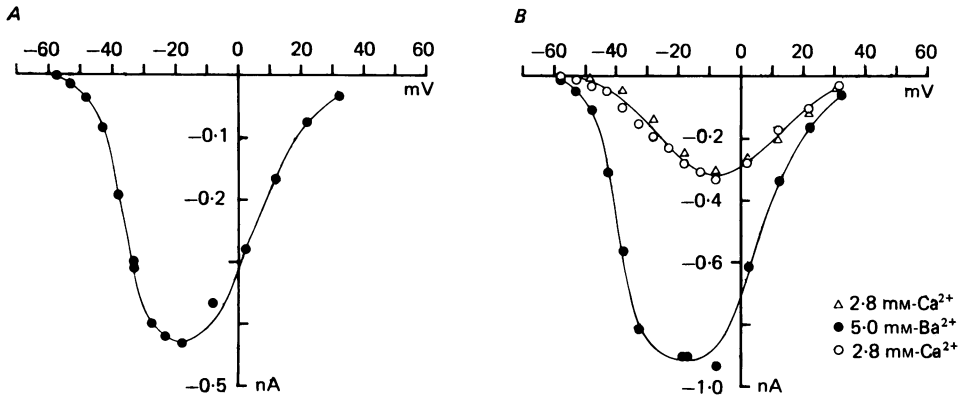

Fig. 13. Current–voltage relationships for the Ba^{2+} current. *A*, inward currents in the presence of external Ba^{2+} for the cell of Fig. 12*A*; measurements made with a normal intracellular medium in the recording electrode. Resonant frequency of cell, 85 Hz. *B*, inward currents obtained with a Cs^{+}-filled electrode: ●, measurements in which 5 mM-Ba^{2+} replaced both external divalent cations; △ and ○, pre- and post-controls in normal extracellular saline, respectively. Holding potential, −68 mV.

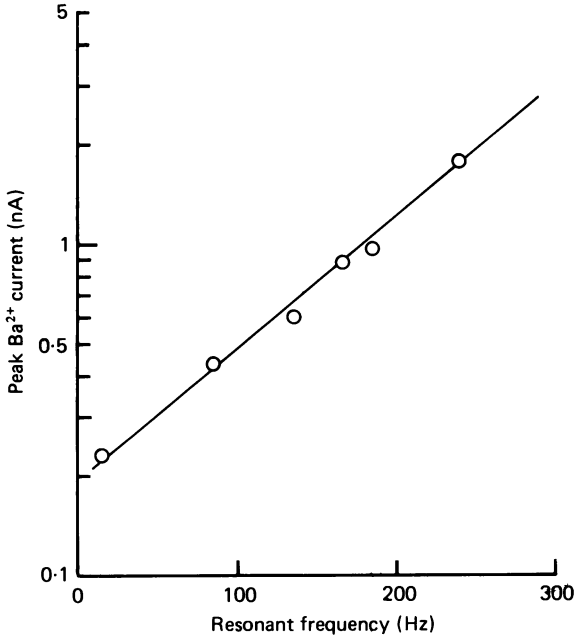

Fig. 14. Plot of the peak inward current in the presence of 5 mM external Ba^{2+} as a function of the hair cell's resonant frequency in six different cells. Line drawn by eye through the points.

The use of Ba^{2+} was itself not without problems, for its effects were often poorly reversible and cells deteriorated after a while in the solution, making it difficult to determine a comprehensive current–voltage curve. Nevertheless, for each of the cells examined, it was feasible to make a series of measurements up to and around the tip of the curve so as to derive a value for the maximum current. The use of Ba^{2+}

abolished the outward K^+ current in cells throughout the frequency range. Measurements of the peak Ba^{2+} current are plotted in Fig. 14 for six cells with resonant frequencies of 13–240 Hz, and the results show a clear systematic increase of this current with resonant frequency. Using a ratio of 3 (Fig. 13*B*) for the relative

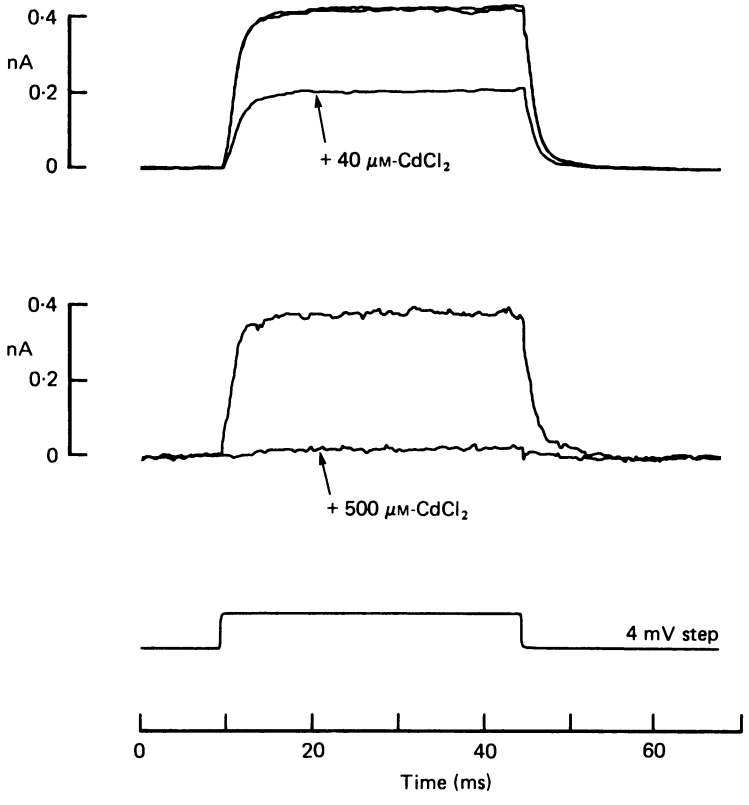

Fig. 15. Effects of external application of $CdCl_2$ on the net outward current in two different hair cells; each set of averaged records are for 4 mV depolarizing steps. In the upper example, the controls before and after Cd^{2+} are superimposed; note that the current was diminished with no effect on its kinetics. In the lower example, there was incomplete recovery following the Cd^{2+} treatment. Holding potentials and resonant frequencies of cells were: upper example, −43 mV, 285 Hz; lower example, −50 mV, 220 Hz.

sizes of Ba^{2+} and Ca^{2+} currents predicts a range of Ca^{2+} currents in these hair cells of 80–600 pA. The range encompasses that obtained with Cs^+-filled electrodes (160–500 pA, $n = 8$) although for those measurements no estimates of resonant frequency were available. In contrast to the Ba^{2+} current's size, its kinetics at a given membrane potential showed no great variation with resonant frequency, and in all cells the activation time constant was less than 1 ms.

Ca^{2+} dependence of K^+ current

Various pharmacological treatments expected to reduce or abolish the Ca^{2+} current were also found to diminish the net current, consistent with the notion advanced previously that the major K^+ conductance in hair cells is a Ca^+-activated one (Lewis

& Hudspeth, 1983*b*; Ohmori, 1984). Such treatments included removal of external Ca^{2+} or addition of millimolar quantities of Co^{2+} or the more effective Cd^{2+}. The effects of two different concentrations of Cd^{2+} are shown in Fig. 15, the lower concentration producing a reversible reduction in the outward current, and the higher concentration virtually abolishing it. It is noteworthy that the low concentration of Cd^{2+} had no influence on the kinetics of the net current, here evoked by a small depolarizing step. In those experiments where the K^+ current was abolished near the resting potential it could be reactivated by larger depolarizing steps that took the membrane potential positive to 0 mV. This is usually interpreted as being due to the intrinsic voltage sensitivity of this type of K^+ channel (Adams, Constanti, Brown & Clarke, 1982; Barrett, Magleby & Pallotta, 1982).

None of these experiments rules out an external action of the divalent ions on the K^+ channel itself and it is necessary to show that direct manipulation of the internal Ca^{2+} will influence the K^+ conductance. Loss of the outward current could also be produced by using BAPTA (Tsien, 1980) rather than EGTA as the Ca^{2+} chelator in the intracellular medium. An advantage of BAPTA is that it has a more rapid equilibration than EGTA, and may thus be a more efficient buffer for internal Ca^{2+} (Marty & Neher, 1985). Preliminary results showed that cells examined with electrodes containing 5 mM-BAPTA displayed no outward current unless they were depolarized beyond about -10 mV, suggesting that the K^+ conductance is normally activated by a modulation in intracellular Ca^{2+}. This conclusion might be more properly examined by perfusing the recording electrode with solutions of different free-Ca^{2+} concentrations buffered by BAPTA, but this was not attempted in the present study.

Current fluctuations

The results so far indicate that of the two major currents flowing in the voltage range around the resting potential, the K^+ current is much the larger and its kinetics are a function of the resonant frequency of the hair cell. One approach to understanding the kinetic processes underlying the gating of the K^+ channel is to characterize the fluctuations in current resulting from the statistical behaviour of these channels. Pronounced current fluctuations could be observed in all cells held in voltage clamp at their resting potential, and the amplitude of the fluctuations was increased by depolarization and decreased by hyperpolarization to a potential where the K^+ conductance would be turned off; the fluctuations were also greatly diminished by application of TEA, implicating the K^+ channels as their source. Examples of the noisiness of the current records are shown in Fig. 16*A* for two cells whose resonant frequencies, given beside each set of traces, are widely spaced. The lower trace of each pair is a sample of membrane current for a 4 mV steady depolarization, and the upper trace is for a hyperpolarization of 25 mV, where the residual activity mostly reflected the instrumentation noise. It is clear from these records that the fluctuations evoked during depolarization had a different spectral composition in the two cells, more high-frequency components being present in the higher-frequency cell.

The power spectral densities of the fluctuations are shown in Fig. 16*B* for these two cells and one other. So as to clearly display the differences between the spectra,

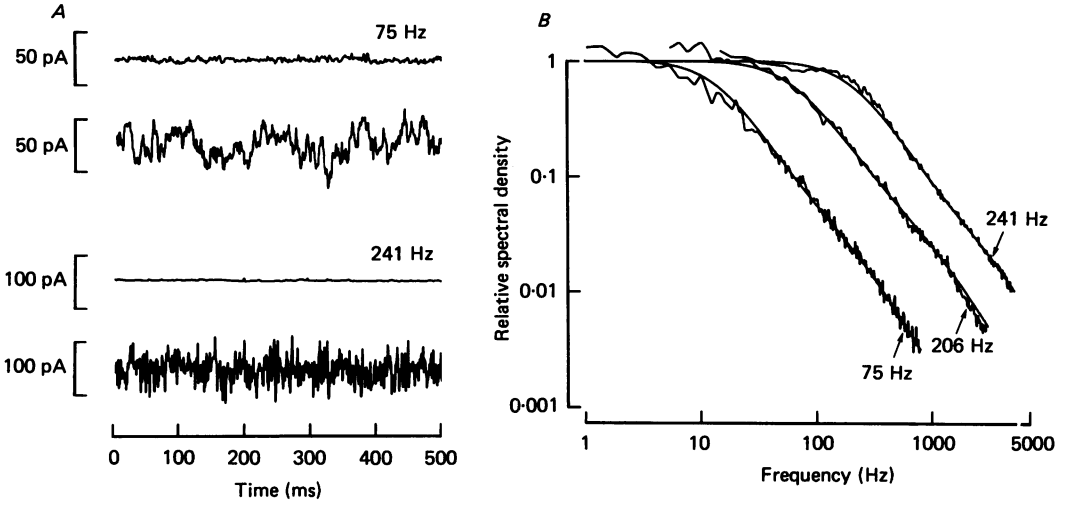

Fig. 16. *A*, membrane current fluctuations in two hair cells of different resonant frequencies, indicated beside the traces. The upper record of each pair was obtained at a holding potential of about −80 mV, and the lower record at a holding potential 4 mV depolarized to the resting potential. All traces filtered with an 8-pole Butterworth low-pass filter at 700 Hz. *B*, spectral densities of the current fluctuations in three cells, whose resonant frequencies are given beside the plots. Each spectrum is the average of the difference between the noise recorded at a holding potential 4 mV positive to the resting potential and that recorded at about −80 mV, which is assumed to reflect the instrumentation noise. The ordinates have been normalized to illustrate that the spectra have similar shapes but are shifted relative to one another along the frequency axis. Resonant frequencies, ordinate scaling factors and number of averages were: 75 Hz, $4{\cdot}5 \times 10^{-24}$ A^2/Hz, 37; 206 Hz, $1{\cdot}1 \times 10^{-24}$ A^2/Hz, 37; 241 Hz, $1{\cdot}2 \times 10^{-24}$ A^2/Hz, 115. The digitization intervals and anti-aliasing filter settings were different for the three spectra. The smooth curves are each the sum of two Lorentzians calculated from eqn. (5) with $f_2/f_1 = 10$. Values of f_1 and $S_2(0)/S_1(0)$ were 19 Hz, 0·02; 88 Hz, 0·022; 300 Hz, 0·017. Temperature, 21–24 °C.

the ordinates have been scaled to make the low-frequency powers comparable; normalizing factors are given in the legend. Each spectrum had a similar over-all form, was roughly flat at low frequencies and declined at higher frequencies with a slope of about $(1/\text{frequency})^{1{\cdot}3}$. However, the frequency at which the roll-off began increased in proportion to the resonant frequency of the cell. The spectral densities (S) were found to be best fitted by the sum of two Lorentzian components, drawn as the smooth curves in Fig. 16*B* and calculated from:

$$S = \frac{S_1(0)}{1+(f/f_1)^2} + \frac{S_2(0)}{1+(f/f_2)^2}, \tag{5}$$

where f is frequency, $S_1(0)$ and $S_2(0)$ are the zero frequency values of the two components and f_1 and f_2 are their respective corner frequencies. For each of the theoretical curves f_2/f_1 was 10 and $S_2(0)/S_1(0)$ was about 0·02. Similar spectra were obtained in three other cells. The corner frequencies (f_1) for the principal spectral component are collected for six cells in Table 2, along with some of their other properties, including the time constant of the current relaxation. The values of the

time constant were roughly comparable to the equivalent time constants ($1/2\pi f_1$) derived from the noise analysis.

The analysis of the fluctuations provides corroborative evidence for the idea that a variation in resonant frequency is associated with changes in the kinetics of gating

TABLE 2. Characteristics of current fluctuations

Cell	Resonant frequency (Hz)	Spectra f_1 (Hz)	Spectra τ_s (ms)	Relaxation τ (ms)	i_0 (pA)
1	75	19	8·4	10	0·99
2	145	64	2·5	3·8	1·13
3	188	122	1·3	1·4	0·87
4	206	88	1·8	2·6	1·08
5	235	300	0·5	1·1	0·63
6	241	323	0·5	1·0	0·76

f_1 is the corner frequency of the principal Lorentzian component of each hair cell's current fluctuations; $\tau_s = (2\pi f_1)^{-1}$. τ in column 5 measured from current relaxations to small positive voltage steps; i_0 is single-channel current estimated from variance-to-mean ratios.

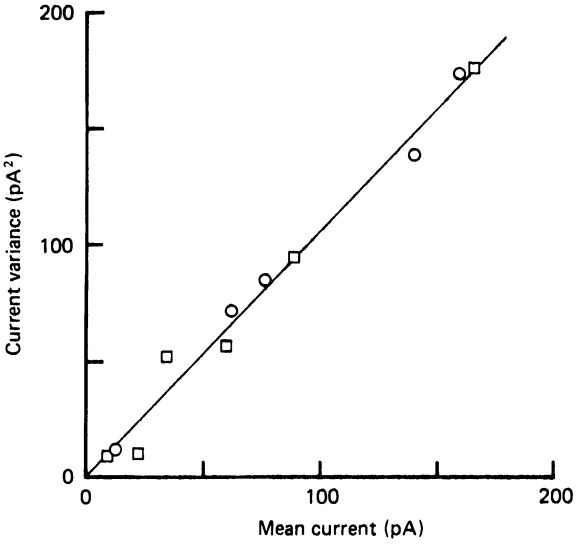

Fig. 17. Variance of the current fluctuations as a function of the mean current level in two hair cells. The measurements were taken at a variety of membrane potentials from −2 to +5 mV relative to the resting potential. Both variance and mean of the current are expressed relative to their values at a holding potential of about −80 mV. Straight line drawn by eye through the points has a slope of 1·06 pA. Resonant frequencies and resting potentials were; ○, 75 Hz, −53 mV; □, 206 Hz, −47 mV.

of the K^+ channel, and further suggests that more than one rate constant may be altered between cells of different frequencies.

Owing to the marked voltage dependence of the K^+ conductance, small voltage excursions around the resting potential were associated with large changes in the current and its variance. A plot of the variance against the net current is presented

for a pair of cells in Fig. 17. The measurements were derived from long voltage-clamp steps of -2 to $+5$ mV, and are referred to the current level and its variance at a holding potential of about -80 mV. For each of the cells, the variance increased in proportion to the mean current, the straight line through the points having a slope of 1 pA. Variance-to-mean ratios for the six cells are given in Table 2, and have an average value of $0{\cdot}9 \pm 0{\cdot}2$ pA. On the assumption that the changes in driving force for the conducting ion are small over the voltage range for which the measurements were taken, the variance (σ^2) and mean current (I) can be related by (Colquhoun & Hawkes, 1977):

$$\sigma^2 = Ii(1-p), \tag{6}$$

where i is the current through a single K^+ channel and p is the probability that it is open; the linear relationship observed between σ^2 and I implies that p was small, and thus the single-channel current, i, was about 1 pA to within experimental error in cells of all resonant frequencies. With a driving force of 30 mV, this current corresponds to a channel conductance of 33 pS. It must be noted that this channel size may not apply to cells of the very lowest frequencies of 10–20 Hz, for which noise measurements were not obtained.

The preceding analyses of the spectral composition of the fluctuations and the current flowing through a single channel have ignored the contributions of the Ca^{2+} current and have assumed that both the variance and the net current are overwhelmingly dominated by the K^+ current. The validity of this approximation could be assessed for one of the cells (cell 4 in Table 2) for which measurements of the Ca^{2+} current were also given and are given in Fig. 10. On adding 25 mM-TEA the current variance at the resting potential for this cell was reduced by a factor of 65 from 116 to 1·8 pA^2, and as was documented above (Fig. 10), the average Ca^{2+} current was about a tenth of that due to K^+. Hence the fluctuation in the Ca^{2+} current would have made a negligible contribution to the over-all variance. Its contribution to the net current would have resulted in a 10 % over-estimate of the current flowing through a single K^+ channel.

Single K^+ channels

In order to confirm that the time course of the macroscopic current resulted from the behaviour of the K^+ channels themselves rather than from some distributed property of the hair cell, such as for example the spatial separation of channels, recordings of single K^+ channels were attempted. These recordings were performed on cell-attached patches. This configuration suffers from the disadvantage that the cells are not properly voltage clamped, though considering their low input resistances, the currents flowing through the patch were unlikely to significantly alter the membrane potential. Also to enhance the signal-to-noise ratio, the recording pipettes were filled with an isotonic K^+ saline.

Two types of step-like current fluctuations indicative of single-channel events were distinguishable in these experiments. One variety had an amplitude of about 1 pA with no applied potential, and it remained open with an increased size for positive voltage steps delivered to the pipette, equivalent to hyperpolarization of the cell; these channels are most likely due to the inward rectifier (Ohmori, 1984). The other variety had a resting amplitude of 3–5 pA and was opened by the equivalent of depolarization. Examples of the latter species are illustrated in Fig. 18, showing the

effects of 20 mV depolarizing steps, and below the single traces are the average time courses of the change in the probability of opening, derived as described in the Methods. Two properties are evident from the Figure: the opening probability of the channel was increased by depolarization and its amplitude was diminished. Current–

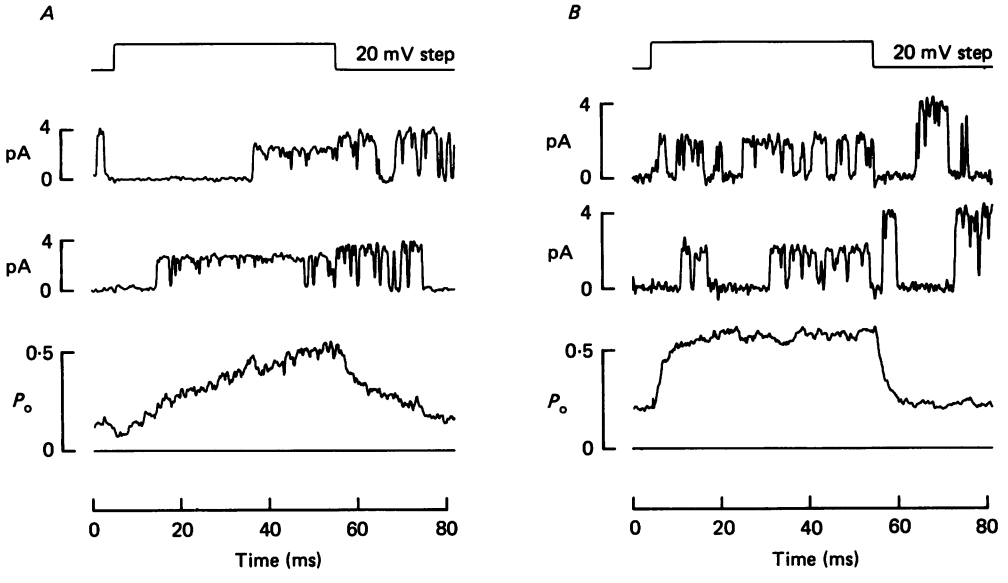

Fig. 18. Single K^+ channel currents recorded from two hair cells. Measurements were made in the cell-attached mode with patch electrodes filled with 134 mM-KCl saline. The top trace shows the timing of the voltage step delivered to the electrode which corresponds to a depolarization of the membrane patch. Middle traces are single records of channel currents which have been filtered with a 6-pole Bessel filter at 3 kHz. The bottom trace gives the ensemble average of the probability (P_0) of the channel being open throughout the stimulus. The number of records averaged was 400 (*A*) and 492 (*B*). The two cells were obtained in different experiments from opposite ends of the cochlea, that of *A* being isolated in dish 1 (see Methods) from the low-frequency apical region, and that of *B* in dish 4 from the high-frequency basal region. Single-channel conductances, estimated from maintained depolarizations and hyperpolarizations were 84 pS (*A*) and 96 pS (*B*).

voltage relationships for the channel were approximately linear, and could be extrapolated to a reversal potential about 50 mV positive to the resting potential, consistent with its being K^+ selective. Since the electrodes were filled with a high-K^+ solution, the K^+ equilibrium potential across the membrane patch would have been close to an absolute potential of 0 mV. The channel conductance ranged from about 70 to 120 pS (mean $\pm$ S.D., 102 ± 14 pS; $n = 8$), a value larger than that inferred from the noise analysis. This discrepancy might be a consequence of the high external K^+ concentration, since it is known that Ca^{2+}-activated K^+ channels in other systems have very different conductances depending on whether the membrane patch is immersed in symmetric or asymmetric salt solutions (Yellen, 1984; Blatz & Magleby, 1984).

Assuming that this type of channel underlies the macroscopic K^+ currents, since it was the only one found to be activated by depolarization in the appropriate voltage

range, then its kinetics might be expected to resemble the macroscopic current. For the two examples illustrated, the open probability rose and fell exponentially with time after the beginning and end of the step; the respective time constants were about 20 ms (Fig. 18*A*) and 2 ms(*B*). Although we had no measure of the resonant frequencies of these cells, they originated from opposite ends of the papilla; the one with slower kinetics was isolated in dish 1 which normally contained the low-frequency cells (see Fig. 2) and that with faster kinetics was isolated into the high-frequency dish 4. The magnitudes of the time constants are roughly consistent with the expected range of resonant frequencies found in these dishes. The results support the notion that the spread in kinetics of the macroscopic K^+ current between cells is due to local variations in the vicinity of each channel, probably resulting in changes in the rate constants of the channel-gating process.

DISCUSSION

Resonance in solitary hair cells

Solitary turtle hair cells displayed all aspects of the resonance phenomenon observed in cells of the intact cochlea, and the spread of their resonant frequencies and the sharpness of tuning add support for the idea that frequency selectivity in the turtle ear is a private property of the hair cells. The lower- and upper-frequency bounds in solitary cells (9–350 Hz) were virtually identical to those found in the isolated papilla (20–320 Hz; Crawford & Fettiplace, 1985) but about an octave down on values obtained by micro-electrode recordings in the intact cochlea, where characteristic frequencies extended up to 700 Hz (Crawford & Fettiplace, 1980). Notable ways in which the first two preparations differed from the last were in the absence of a tectorial membrane attachment for the ciliary bundles, and the exposure of the bundles to perilymph rather than the normal ionic environment of endolymph. The end result of these differences might have been a reduction in the transducer conductance, though it is unclear how this relates to the resonance. As mentioned earlier, loss of the transducer current could account for the tendency of some cells to be hyperpolarized away from where they were most highly tuned. Despite these small differences, the distribution of tuning characteristics in solitary cells reasonably approximated that of the intact organ, and motivated our subsequent search for possible variations in the underlying membrane conductances.

Membrane currents

Two major ionic currents, one carried by K^+ and the other by Ca^{2+} that have been described in hair cells of the frog (Lewis & Hudspeth, 1983*b*) and chick (Ohmori, 1984) were also present in the turtle; both were activated by depolarization in the voltage range around the resting potential where the resonance behaviour is most prominent (Fig. 10*A*). In addition, isolated turtle hair cells have been shown to transduce mechanical stimuli delivered to the ciliary bundle (Art *et al.* 1986*b*), maximum transducer currents up to 200 pA being observed.

Of the two major voltage-dependent currents, the K^+ current was much the larger, and in a majority of cells was blocked by TEA at a concentration that would extinguish the resonance behaviour on current injection (Crawford & Fettiplace,

1981*b*; Art *et al.* 1985). Both the size and the speed of the current were found to increase systematically with the resonant frequency of the cell, the kinetics showing the greatest variation. Taken together, these observations argue that the K^+ current plays a major role in generating the resonance, a conclusion also reached for frog saccular hair cells (Lewis & Hudspeth, 1983*b*; Lewis, 1985).

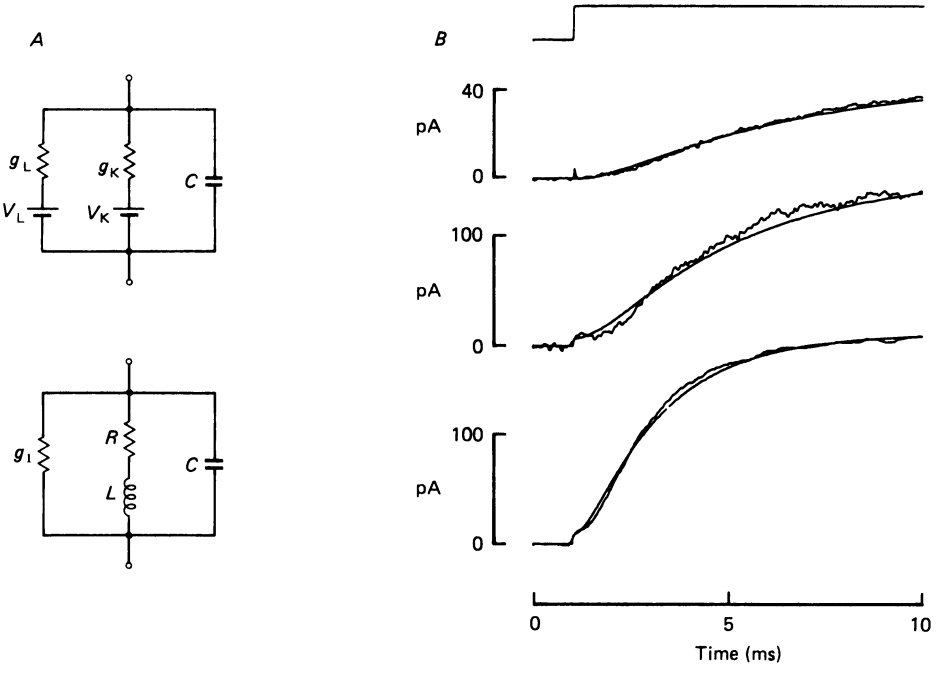

Fig. 19. *A*, equivalent circuits used to predict resonance behaviour of hair cells. Hair cell membrane is assumed to contain a voltage-sensitive K^+ conductance, g_K, and a leak conductance, g_L, in parallel with the membrane capacitance, C. If g_K activates with a single time constant, the membrane is equivalent to the lower circuit, where L and R are given by eqns. (2*a*) and (11), and g_1 includes contributions from both g_K and g_L. V_K and V_L are the K^+ and leak equilibrium potentials, respectively. *B*, net current responses for 2 mV depolarizing steps, illustrating sigmoidal onsets, for cells 2, 3 and 4 in Table 3. Smooth curves calculated as the sum of a time-dependent component (given by eqn. (13) with $\tau_1/\tau_2 = 5$), and an instantaneous component representing the current flowing through the shunt conductance, g_1. Note that the experimental records show more of a delay than is predicted by the second-order system.

Prediction of resonant frequencies

In the following analysis we shall assess the extent to which the magnitude and kinetics of the K^+ conductance can account for the resonant frequencies observed experimentally. The Ca^{2+} current will, as a first approximation, be neglected and the K^+ conductance will be regarded as purely voltage sensitive. Two schemes are considered to describe its activation kinetics.

First-order kinetics

With first-order kinetics it has been shown (Detwiler *et al.* 1980; Ashmore & Attwell, 1985) that, for small perturbations in membrane potential, the voltage-

dependent conductance, g_K, can behave like an inductance, L, coupled to a pair of resistances. Therefore the equivalent circuit for the membrane including the cell capacitance, C, is that shown in the lower half of Fig. 19*A* (Crawford & Fettiplace, 1981*a*). The value of the inductance is given by:

$$L = \frac{\tau}{\frac{\partial g_K}{\partial V}(V - V_K)}, \tag{2a}$$

where τ is the activation time constant and V_K, the K^+ equilibrium potential, is negative to the membrane potential, V, at rest.

The dependence of the conductance, g_K, on membrane potential was obtained from the tail-current measurements (Fig. 7) and near the resting potential could be approximated by:

$$g_K = A \exp(V/V_E), \tag{7}$$

where A and V_E are constants, and V_E, representing the steepness of the voltage-dependence, had a mean value of 3·2 mV. Thus the denominator in eqn. (2*a*) becomes:

$$\frac{\partial g_K}{\partial V}(V - V_K) = \frac{pI_{max}}{V_E}, \tag{8}$$

where I_{max} is the saturating amplitude of the tail current, and p the fraction turned on at rest, which in most cells lay between 0·1 and 0·3.

The impedance, Z, of the equivalent circuit as a function of angular frequency, ω, is given by:

$$Z(\omega) = \frac{R\left[1 + \left(\frac{\omega Q_0}{\omega_0}\right)^2\right]^{\frac{1}{2}}}{\left\{\left[1 + g_1 R - \left(\frac{\omega}{\omega_0}\right)^2\right]^2 + \left(\frac{\omega Q_0}{\omega_0}\right)^2\left[\frac{1}{Q_0^2} + g_1 R\right]^2\right\}^{\frac{1}{2}}}, \tag{9}$$

where R is the resistance and g_1 the parallel shunt conductance in the lower half of Fig. 19*A*, and ω_0 and Q_0 are functions of the circuit parameters. The values of these constants could be obtained directly from tail-current measurements on each cell:

$$\omega_0^2 = \frac{1}{LC} = \frac{pI_{max}}{C\tau V_E}, \tag{10}$$

$$R = \frac{L}{\tau} = \frac{V_E}{pI_{max}}, \tag{11}$$

$$Q_0^2 = \frac{L}{R^2 C} = \frac{\tau pI_{max}}{CV_E}. \tag{12}$$

In the real membrane the parallel shunt conductance will be a combination of an instantaneous K^+ component plus contributions from the Ca^{2+} current and leak, so we derived values for parallel shunt conductance in each cell from measurements of the initial hump at the onset of the current response (see Fig. 19*B*). The resonance curve was then calculated from eqn. (9): the resonant frequency, f_0, was derived from the frequency at maximum impedance and the quality factor, Q, from f_0 and the 3 dB band width (b.w.) of the curve ($Q = f_0$/b.w.). For all but the very lowest-frequency cells, the predicted resonant frequency values were 10–20 % too high, and the quality factor was much too small, always less than 2·6. The poor tuning that results from

a single voltage-dependent conductance with first-order kinetics has been stressed by Ashmore & Attwell (1985), who showed that a much sharper resonance peak was achieved with a conductance that activated with an extra delay.

Second-order kinetics

The introduction of an additional delay is applicable to our results and is consistent both with the sigmoidal current onsets and with the spectral composition of the current fluctuations. A scheme incorporating two delays might be rationalized in terms of a channel with three kinetic states: two closed states with and without bound Ca^{2+} and an open state also complexed to Ca^{2+}. The step response of the second-order system for initial (I_0) and final (I_∞) values of the current, I, is given by:

$$I(t) = I_\infty - \frac{I_\infty - I_0}{\tau_2 - \tau_1}(\tau_2 \, e^{-t/\tau_2} - \tau_1 \, e^{-t/\tau_1}). \tag{13}$$

This equation gave an acceptable fit to the rising phase of the current at the start of a small voltage-clamp step (see Fig. 19*B*), with τ_1, the principal time constant being about five times τ_2, the second time constant; in some cells, superior fits were produced by employing two fast time constants and one slower one. Second-order kinetics will account for the form of the spectral density curves (Fig. 16*B*) which fell off as the sum of two Lorentzian components with corner frequencies given by $(2\pi\tau_1)^{-1}$ and $(2\pi\tau_2)^{-1}$. Power spectra of this form have also been reported for a molluscan Ca^{2+}-activated K^+ conductance (Hermann & Hartung, 1982).

Although the membrane is no longer equivalent to the circuit in Fig. 19, its impedance, Z, can be expressed in a similar form to eqn. (9), as shown by Ashmore & Attwell (1985):

$$Z(\omega) = \frac{R\left[1+\left(\frac{\omega Q_0}{\omega_0}\right)^2\right]^{\frac{1}{2}}}{\left\{\left[g_1 R - \left(\frac{\omega}{\omega_0}\right)^2 + \frac{1}{1+\omega^2\tau_2^2}\right]^2 + \left(\frac{\omega}{\omega_0}\right)^2\left[\frac{1}{Q_0} + g_1 R Q_0 - \frac{\omega\tau_2}{1+\omega^2\tau_2^2}\right]^2\right\}^{\frac{1}{2}}}, \tag{14}$$

where parameters have the same values as for the conductance with first-order kinetics. This equation reduces to eqn. (9) if τ_2 is set to zero. With τ replaced by τ_1, eqns. (10)–(12) and (14) were used to predict the resonance curves in a collection of hair cells, and in each case values for p, V_E and I_{max} were derived from tail-current measurements. The resonant frequency and quality factor were obtained from the calculated tuning curves, and are given in Table 3 along with some relevant experimental parameters.

There is reasonable agreement between the experimental and theoretical values for the resonant frequency, and for all cells, the model predicts sharp tuning as reflected in the high quality factors. For the very lowest-frequency (17 Hz) cell, no second time constant was needed since the current built up as a single exponential (Fig. 5); for other cells the second time constant was initially chosen to be a fifth of the principal time constant, which itself was obtained from the relaxation of the tail current. However, for the highest-frequency cell in Table 3, somewhat better agreement between experiment and theory was achieved by allowing the second time constant to have a minimum value of 0·3 ms, which might be rationalized as the limit set by the kinetics of the Ca^{2+} current.

The scheme employed does not provide a complete description of the membrane currents in turtle hair cells, but it is the simplest one consistent with the kinetics of the K^+ conductance which can generate sharp tuning. Therefore it is useful in indicating how the characteristics of the K^+ conductance may be important in

TABLE 3. Measured and predicted tuning in six hair cells

	Measured							Predicted	
Cell	f_0 (Hz)	Q	C (pF)	I_{max} (pA)	τ_1 (ms)	τ_2 (ms)	g_1R	f_0 (Hz)	Q
1	17	4·6	10	639	138	—	0·01	17	4·3
2	67	8·2	11·3	480	7·5	1·5	0·03	64	10·7
3	145	12·6	10	925	3·8	0·8	0·06	141	17·6
4	206	31·0	12·5	1200	2·6	0·5	0·07	242	34·6
5	276	13·7	15	2336	1·2	0·3	0·08	280	6·5
6	309	14·0	10·6	1200	0·9	0·2	0·03	333	6·1
						0·3	0·03	312	17·3

Resonant frequency, f_0, and quality factor, Q: measured values in first two columns and predicted values (from eqn. (14)) in last two columns. C, cell capacitance; I_{max}, saturated tail current; τ_1, principal time constant of current relaxation. g_1 (parallel shunt conductance) was measured and R (resistance) calculated from eqn. (11). The last cell had an anomalously small I_{max}, but was included because of its high quality factor.

determining the resonant frequency. No explicit account has been taken of the Ca^{2+} current, and a more detailed analysis of the interplay of the two membrane currents would require a model such as that proposed by Lewis (1985) for the complex gating process of the K^+ channel.

Kinetics of the K^+ current

One of our main observations was the wide range of time constants with which the K^+ current activates. The simplest explanation is that the variation reflects intrinsic differences in the K^+ channels. If however these channels are gated by modulation of internal Ca^{2+}, then the rate of entry and buffering of Ca^{2+} within the cell could also contribute to the kinetic variation. Activation of the Ca^{2+} current was faster than the fastest relaxation time constant measured for the K^+ current and cannot therefore determine the over-all kinetics in the frequency range examined. If the relationship between the relaxation time constant and resonant frequency shown in Fig. 6*B* extends to higher frequencies, the kinetics of the Ca^{2+} current, if they were to remain constant, would dominate above 500 Hz. This frequency is close to the upper limit for the resonance in turtle hair cells at room temperature.

Additional information on the kinetic processes was provided by analysis of the current fluctuations, whose major spectral component varied in parallel with the relaxation time constant. We have argued that the Ca^{2+} channel noise would have been small and it seems unlikely that the internal Ca^{2+} buffering mechanisms are intrinsically noisy, since they arise from binding to cytoplasmic proteins or membrane pumps. Therefore it is most reasonable to suppose that the current noise is largely due to the probabilistic behaviour of the K^+ channels, and that differences in the major spectral component reflect differences in the opening and closing rate constants

of the channel. Some support for this conclusion was provided by direct measurement of the kinetics of single K^+ channels (Fig. 18).

Density of K^+ channels

The fluctuation analysis indicated a single-channel current of about 1 pA at least for resonant frequencies above 75 Hz. If the channels exhibit fast flickering undetectable within the band width of the recording system, this value may be an underestimate (Colquhoun & Hawkes, 1977), but taking it to be correct allows a calculation of the number of K^+ channels per hair cell. The saturating value of the tail current in Fig. 10*A* (1·2 nA) represents the maximum current flowing through the open channels for a driving force at the resting potential. From Fig. 10, the tail current had saturated at a membrane potential where the Ca^{2+} current was still increasing, and cannot therefore be limited by Ca^{2+} influx. If we assume that at saturation the probability of channel opening is close to unity, then we calculate about 1200 channels for that cell; estimations in other cells (Fig. 7 and Table 3), gave numbers ranging from about 480 to 3700 K^+ channels per cell. Since there was no systematic variation of membrane area with resonant frequency, our results show that, in general, cells of a higher resonant frequency had a higher density of channels in their membrane. Such estimates do not include the population of cells with the very lowest resonant frequencies (10–20 Hz), for which no reliable measurements of the single-channel current were available.

An intriguing question that remains is how the hair cells regulate the number and kinetics of their K^+ channels, and the number of Ca^{2+} channels. The cells are arranged tonotopically in the epithelium, the resonant frequency increasing monotonically with distance along the cochlea (Crawford & Fettiplace, 1980; Art *et al.* 1986*a*), which implies that the membrane properties are graded with position, just as are the cellular dimensions in other cochleas (Lim, 1980; Tilney & Saunders, 1983). While the cellular architecture may be initially set by gene expression, it seems likely that the properties of the channel proteins, if these proteins turn over, require continual management to preserve the precise geographical distribution of resonant frequencies along the cochlea.

This research was supported by grants from the Medical Research Council and the Howe Fund of the Royal Society. We would like to thank Paul Fuchs, who participated in early experiments, Andrew Crawford for helpful discussions and Trevor Lamb and Brian Nunn for commenting on the manuscript. We acknowledge the technical assistance of W. Smith and T. Carter and thank Dr S. K. Bosher for loan of equipment.

REFERENCES

ADAMS, P. R., CONSTANTI, A., BROWN, D. A. & CLARK, R. B. (1982). Intracellular Ca^{2+} activates a fast voltage-sensitive K^+ current in vertebrate sympathetic neurones. *Nature* **296**, 746–749.

ALDRICH, R. W. & YELLEN, G. (1983). Analysis of nonstationary channel kinetics. In *Single-channel Recording*, ed. SAKMANN, B. & NEHER, E., pp. 287–299. New York: Plenum Press.

ART, J. J., CRAWFORD, A. C. & FETTIPLACE, R. (1986*a*). Electrical resonance and membrane currents in turtle cochlear hair cells. *Hearing Research* **22**, 31–36.

ART, J. J., CRAWFORD, A. C. & FETTIPLACE, R. (1986*b*). Membrane currents in solitary turtle hair cells. In *Auditory Frequency Selectivity*, ed. MOORE, B. C. J. & PATTERSON, R. D., pp. 81–88. New York: Plenum Press.

ART, J. J., CRAWFORD, A. C., FETTIPLACE, R. & FUCHS, P. A. (1985). Efferent modulation of hair cell tuning in the cochlea of the turtle. *Journal of Physiology* **360**, 397–421.

ASHCROFT, F. M. & STANFIELD, P. R. (1982). Calcium inactivation in skeletal muscle fibres of the stick insect *Carausius morosus*. *Journal of Physiology* **330**, 349–372.

ASHMORE, J. F. (1983). Frequency tuning in a frog vestibular organ. *Nature* **304**, 536–538.

ASHMORE, J. F. & ATTWELL, D. (1985). Models for electrical tuning in hair cells. *Proceedings of the Royal Society* B **226**, 325–344.

ASHMORE, J. F. & PITCHFORD, S. (1985). Evidence for electrical tuning in hair cells of the frog amphibian papilla. *Journal of Physiology* **364**, 39*P*.

BARRETT, J. N., MAGLEBY, K. L. & PALLOTTA, B. S. (1982). Properties of single calcium-activated potassium channels in cultured rat muscle. *Journal of Physiology* **331**, 221–230.

BENDAT, J. S. & PIERSOL, A. G. (1971). *Random Data: Analysis and Measurement Procedures*. New York: Wiley–Interscience.

BLATZ, A. L. & MAGLEBY, K. L. (1984). Ion conductance and selectivity of single calcium-activated potassium channels in cultured rat muscle. *Journal of General Physiology* **84**, 1–23.

COLQUHOUN, D. & HAWKES, A. G. (1977). Relaxation and fluctuations of membrane currents that flow through drug-operated ion channels. *Proceedings of the Royal Society* B **199**, 231–262.

COREY, D. P. & HUDSPETH, A. J. (1979). Ionic basis of the receptor potential in a vertebrate hair cell. *Nature* **281**, 675–677.

CRAWFORD, A. C. & FETTIPLACE, R. (1980). The frequency selectivity of auditory nerve fibres and hair cells in the cochlea of the turtle. *Journal of Physiology* **306**, 79–125.

CRAWFORD, A. C. & FETTIPLACE, R. (1981*a*). An electrical tuning mechanism in turtle cochlear hair cells. *Journal of Physiology* **312**, 377–412.

CRAWFORD, A. C. & FETTIPLACE, R. (1981*b*). Non-linearities in the responses of turtle hair cells. *Journal of Physiology* **315**, 317–338.

CRAWFORD, A. C. & FETTIPLACE, R. (1985). The mechanical propeties of ciliary bundles of turtle cochlear hair cells. *Journal of Physiology* **364**, 359–379.

DETWILER, P. B., HODGKIN, A. L. & MCNAUGHTON, P. A. (1980). Temporal and spatial characteristics of the voltage response of rods in the retina of the snapping turtle. *Journal of Physiology* **300**, 213–250.

ECKERT, R. & CHAD, J. E. (1984). Inactivation of Ca channels. *Progress in Biophysics and Molecular Biology* **44**, 215–267.

FENWICK, E., MARTY, A. & NEHER, E. (1982). Sodium and calcium channels in bovine chromaffin cells. *Journal of Physiology* **331**, 599–635.

FUCHS, P. A. & MANN, A. C. (1986). Voltage oscillations and ionic currents in hair cells isolated from the apex of the chick's cochlea. *Journal of Physiology* **371**, 31*P*.

GORMAN, A. L. F., HERMANN, A. & THOMAS, M. V. (1982). Ionic requirements for membrane oscillations and their dependence on the calcium concentration in a molluscan pace-maker neurone. *Journal of Physiology* **327**, 185–217.

HAGIWARA, S. & OHMORI, H. (1982). Studies of calcium channels in rat clonal pituitary cells with patch electrode voltage clamp. *Journal of Physiology* **331**, 231–252.

HAMILL, O. P., MARTY, A., NEHER, E., SAKMANN, B. & SIGWORTH, F. J. (1981). Improved patch-clamp techniques for high-resolution current recording from cells and cell-free membrane patches. *Pflügers Archiv* **391**, 85–100.

HERMANN, A. & HARTUNG, K. (1982). Noise and relaxation measurements of the Ca^{++}-activated K^+ current in *Helix* neurones. *Pflügers Archiv* **393**, 254–261.

KRISHTAL, O. A. & PIDOPLICHKO, V. I. (1980). A receptor for protons in the nerve cell membrane. *Neuroscience* **5**, 2325–2327.

LAMB, T. D. (1983). An inexpensive perfusion pump and its use in rapid temperature change experiments on retinal rods. *Journal of Physiology* **332**, 7*P*.

LEWIS, R. S. (1985). The ionic basis of frequency selectivity in hair cells of the bullfrog's sacculus. Ph.D. Thesis, California Institute of Technology, Pasadena, CA, U.S.A.

LEWIS, R. S. & HUDSPETH, A. J. (1983*a*). Frequency tuning and ionic conductances in hair cells of the bullfrog's sacculus. In *Hearing – Physiological Bases and Psychophysics*, ed. KLINKE, R. & HARTMANN, R., pp. 17–22. Berlin and Heidelberg: Springer-Verlag.

LEWIS, R. S. & HUDSPETH, A. J. (1983*b*). Voltage- and ion-dependent conductances in solitary vertebrate hair cells. *Nature* **304**, 538–541.

LIM, D. J. (1980). Cochlear anatomy related to cochlear micromechanics. A review. *Journal of the Acoustical Society of America* **67**, 1686–1695.

MARTY, A. & NEHER, E. (1983). Tight-seal whole-cell recording. In *Single-channel Recording*, ed. SAKMANN, B. & NEHER, E., pp. 107–122. New York: Plenum Press.

MARTY, A. & NEHER, E. (1985). Potassium channels in cultured bovine adrenal chromaffin cells. *Journal of Physiology* **367**, 117–141.

MAURO, A., CONTI, F., DODGE, F. & SCHOR, R. (1970). Subthreshold behavior and phenomenological impedance of the squid giant axon. *Journal of General Physiology* **55**, 497–523.

MILLER, M. R. (1978). Scanning electron microscope studies of the papilla basilaris of some turtles and snakes. *American Journal of Anatomy* **151**, 409–436.

OHMORI, H. (1984). Studies of ionic currents in the isolated vestibular hair cell of the chick. *Journal of Physiology* **350**, 561–581.

SIGWORTH, F. J. (1983). Electronic design of the patch clamp. In *Single-channel Recording*, ed. SAKMANN, B. & NEHER, E., pp. 3–35. New York: Plenum Press.

TILNEY, L. G. & SAUNDERS, J. C. (1983). Actin filaments, stereocilia, and hair cells of the bird cochlea. I. Length, number, width and distribution of stereocilia on each hair cell are related to the position of the hair cell on the cochlea. *Journal of Cell Biology* **96**, 807–821.

TSIEN, R. Y. (1980). New calcium indicators and buffers with high selectivity against magnesium and protons: design, synthesis, and properties of prototype structures. *Biochemistry* **19**, 2396–2404.

YELLEN, G. (1984). Ionic permeation and blockade in Ca^{2+}-activated K^+ channels of bovine chromaffin cells. *Journal of General Physiology* **84**, 157–186.

ZUCKER, R. S. (1981). Tetraethylammonium contains an impurity which alkalizes cytoplasm and reduces calcium buffering in neurons. *Brain Research* **208**, 473–478.

EXPLANATION OF PLATE

Photomicrograph of a solitary hair cell isolated from the middle region of the turtle basilar papilla and viewed with Nomarski optics. Note the prominent cuticular plate beneath the stereociliary bundle.


10 μM